WILLIAM & MARY
CHARTERED 1693

W&M ScholarWorks

Arts & Sciences Articles

Arts and Sciences

2013

Mass of the b quark from lattice NRQCD and lattice perturbation theory

A. J. Lee

C. J. Monahan

R. R. Horgan

C. J. Monahan
William & Mary, cjmonahan@wm.edu

Follow this and additional works at: https://scholarworks.wm.edu/aspubs

Mass of the *b* quark from lattice NRQCD and lattice perturbation theory

A. J. Lee,[1] C. J. Monahan,[1,2] R. R. Horgan,[1] C. T. H. Davies,[3] R. J. Dowdall,[1,3] and J. Koponen[3]

(HPQCD Collaboration)[*]

[1]*Department of Applied Mathematics and Theoretical Physics, University of Cambridge,
Centre for Mathematical Sciences, Cambridge CB3 0WA, United Kingdom*
[2]*Physics Department, College of William and Mary, Williamsburg, Virginia 23187, USA*
[3]*SUPA, School of Physics and Astronomy, Kelvin Building, University of Glasgow, Glasgow G12 8QQ, Scotland*
(Received 19 February 2013; published 19 April 2013)

We present a determination of the *b*-quark mass accurate through $\mathcal{O}(\alpha_s^2)$ in perturbation theory and including partial contributions at $\mathcal{O}(\alpha_s^3)$. Nonperturbative input comes from the calculation of the Υ and B_s energies in lattice QCD, including the effect of *u*, *d* and *s* sea quarks. We use an improved NRQCD action for the *b* quark. This is combined with the heavy quark energy shift in NRQCD determined using a mixed approach of high-β simulation and automated lattice perturbation theory. Comparison with experiment enables the quark mass to be extracted: in the $\overline{\text{MS}}$ scheme we find $\overline{m}_b(\overline{m}_b) = 4.166(43)$ GeV.

I. INTRODUCTION

The accurate determination of quark masses is an important component of high-precision tests of the Standard Model. Because quarks cannot be isolated experimentally, the mass must be defined carefully, and its extraction from quantities that are accessible to experiment must be well controlled from the theory side. The *b*-quark mass is particularly important: its uncertainty feeds into errors in tests of the Standard Model in B physics as well as into the cross section for the Higgs decay, $H \rightarrow b\bar{b}$.

The most accurate results to date for the *b*-quark mass come from comparison of the experimental cross section for e^+e^- to hadrons in the bottomonium region with high-order (α_s^3) continuum QCD perturbation theory [1–3]. Errors of 0.5% are possible. A similar method has now been applied to lattice QCD results [4,5], using pseudo-scalar correlators made from heavy quarks instead of the experimental cross section. For these calculations, the experimental input is the value of the meson mass (in this case the η_b) used to tune the lattice *b*-quark mass. Again a 0.5% error is achieved, and good agreement is seen with the continuum results.

It is important to test these determinations against a different method of obtaining the *b*-quark mass which has completely uncorrelated systematic errors. This is the aim of the present paper. We use a direct determination from full lattice QCD calculations of the binding energy of both Υ and B_s mesons. Since we use a nonrelativistic effective theory for the *b* quark (NRQCD) [6,7] this needs a calculation of the heavy quark energy shift. We do this in lattice QCD perturbation theory through two loops (with partial three-loop contributions), significantly improving

on earlier determinations that used one-loop calculations [8]. We have also implemented a one-loop improved NRQCD action to reduce systematic errors.

Calculating higher-order loop corrections in lattice perturbation theory for heavy quarks in NRQCD grows ever more difficult with each order, owing to the increasing number of diagrams and the complicated vertex structure. Various authors [9–11] have suggested an approach in which the heavy quark propagator is measured in the weak coupling regime and the renormalization parameters are fitted to a polynomial in α_s, thus obtaining the radiative corrections beyond one loop. This method is certainly practical for obtaining the quenched contributions to renormalization parameters since quenched gauge configurations are relatively cheap to generate. At two-loop order there are relatively few remaining diagrams with sea quark loops, and these can be feasibly computed using automated lattice perturbation theory. In contrast, there are many two-loop diagrams containing only gluon propagators that pose a challenging task for direct evaluation with automated lattice perturbation theory. We therefore employ a mixed approach to the determination of the two-loop heavy quark energy shift, combining quenched high-β calculations with automated lattice perturbation theory for the sea quark pieces.

In Sec. II we discuss how we extract the *b*-quark mass from simulations of lattice NRQCD. Section III A describes the automated lattice perturbation theory computation of the fermionic contributions to the two-loop energy shift. We present our implementation of the high-β method in Sec. III B, including the concomitant finite volume perturbation theory in Appendix A. The details of the standard nonperturbative part of the calculation are given in Sec. IV. Finally we detail the extraction of the $\overline{\text{MS}}$ mass in Sec. V and present our conclusions in Sec. VII.

---

[*]http://www.physics.gla.ac.uk/HPQCD

II. EXTRACTING THE *b*-QUARK MASS

Quark confinement ensures that quark masses are not physically measurable quantities, so the notion of quark mass is a theoretical construction. A wide range of quark mass definitions exist, often tailored to exploit the physics of a particular process. One common choice of quark mass is the pole mass, defined as the pole in the renormalized heavy quark propagator. The pole mass, however, is a purely perturbative concept and suffers from infrared ambiguities known as renormalons [12,13]. A better mass is the running mass in the $\overline{\text{MS}}$ scheme, which is free of renormalon ambiguities by construction, and is the usual choice for quoting the quark masses. Lattice calculations use the renormalon-free bare lattice mass, which must then be matched to $\overline{\text{MS}}$ to enable a meaningful comparison. We match bare lattice quantities to the $\overline{\text{MS}}$ mass using the pole mass as an intermediate step. Any renormalon ambiguities cancel in the full matching procedure between the lattice quantities and the $\overline{\text{MS}}$ mass, as we argue below. For an explicit demonstration, see [14].

A. Extracting the pole mass

We determine the heavy quark pole mass M_{pole} by relating it to the experimental Υ mass $M_{\Upsilon}^{\text{expt}}$. The mass of a heavy meson is given by twice the pole quark mass plus the binding energy. In an effective theory such as NRQCD, physics above the scale of the *b*-quark mass is removed and the origin of energy for the heavy quark is shifted by E_0, leading to the relation [15]

$$2M_{\text{pole}} = M_{\Upsilon}^{\text{expt}} - a^{-1}(aE_{\text{sim}} - 2aE_0). \tag{1}$$

Here E_{sim} is the energy of the Υ meson at zero momentum, extracted from lattice NRQCD data at lattice spacing a. The quantity $(E_{\text{sim}} - 2E_0)$ corresponds to the "binding energy" of the meson in NRQCD, and we must determine E_0 perturbatively in order to find M_{pole}. With our NRQCD action, we can also calculate the pole mass using the B_s meson,

$$M_{\text{pole}} = M_{B_s}^{\text{expt}} - a^{-1}(aE_{\text{sim}}^{B_s} - aE_0). \tag{2}$$

We use this as a check for systematic errors, which could be quite different in heavy-heavy and heavy-light systems.

In principle, one could extract the quark mass by directly matching the pole mass to the bare lattice NRQCD mass in physical units, m_0, via the heavy quark mass renormalization Z_{m_0},

$$M_{\text{pole}} = Z_{m_0}(am_0)m_0. \tag{3}$$

We found, however, that extracting a sufficiently precise quenched two-loop mass renormalization from high-β simulations was not possible with the statistics available. In this paper, we therefore discuss only the energy shift method.

B. Matching the pole mass to the $\overline{\text{MS}}$ mass

The mass renormalization relating the pole mass to the $\overline{\text{MS}}$ mass, $\overline{m}_b$, evaluated at some scale μ, is given by

$$\overline{m}_b(\mu) = Z_M^{-1}(\mu)M_{\text{pole}}, \tag{4}$$

and has been calculated to three loops in [16].

Although the pole mass is plagued by renormalon ambiguities, these cancel when lattice quantities are related to the $\overline{\text{MS}}$ mass. This can be seen by equating Eqs. (1) and (3) and rearranging them to obtain

$$2(Z_{m_0}m_0 - E_0) = M_{\Upsilon}^{\text{expt}} - E_{\text{sim}}. \tag{5}$$

The two quantities on the right-hand side of the equation are renormalon-ambiguity-free: $M_{\Upsilon}^{\text{expt}}$ is a physical quantity and E_{sim} is determined nonperturbatively from lattice simulations. Any renormalon ambiguities in the two power series Z_{m_0} and E_0 on the left-hand side of the equation must therefore cancel at every order in α_s. This renormalon cancellation is also evident in the direct matching of the bare lattice mass to the $\overline{\text{MS}}$ mass,

$$\overline{m}_b(\mu) = Z_{m_0}(am_0)Z_M^{-1}(\mu)m_0, \tag{6}$$

as both $\overline{m}_b$ and m_0 are renormalon-free.

We combine Eqs. (1) and (4) to relate lattice quantities to the $\overline{\text{MS}}$ mass,

$$\overline{m}_b(\mu) = \frac{1}{2}Z_M^{-1}(\mu)[M_{\Upsilon}^{\text{expt}} - a^{-1}(aE_{\text{sim}} - 2aE_0)], \tag{7}$$

and similarly for the B_s meson,

$$\overline{m}_b(\mu) = Z_M^{-1}(\mu)[M_{B_s}^{\text{expt}} - a^{-1}(aE_{\text{sim},B_s} - aE_0)]. \tag{8}$$

These relations will be used to extract $\overline{m}_b(\overline{m}_b)$ once we have calculated E_0 and E_{sim}, which we describe in detail in the next sections.

C. NRQCD, gluon and light quark actions

We now describe the heavy quark, gluon and light quark actions used in our calculation. We use the Symanzik-improved $\mathcal{O}(v^4)$ NRQCD action, given in [8,17], which has already been successfully used by HPQCD in a number of heavy quark physics calculations; see, e.g., [8,17–21]. The Hamiltonian is given by

$$aH = aH_0 + a\delta H, \tag{9}$$

$$aH_0 = -\frac{\Delta^{(2)}}{2am_0}, \tag{10}$$

$$a\delta H = -c_1\frac{(\Delta^{(2)})^2}{8(am_0)^3} + c_2\frac{ig}{8(am_0)^2}(\nabla \cdot \tilde{\mathbf{E}} - \tilde{\mathbf{E}} \cdot \nabla)$$
$$- c_3\frac{g}{8(am_0)^2}\sigma \cdot (\tilde{\nabla} \times \tilde{\mathbf{E}} - \tilde{\mathbf{E}} \times \tilde{\nabla})$$
$$- c_4\frac{g}{2am_0}\sigma \cdot \tilde{\mathbf{B}} + c_5\frac{a^2\Delta^{(4)}}{24am_0} - c_6\frac{a(\Delta^{(2)})^2}{16n(am_0)^2}. \tag{11}$$

$\Delta^{(2)}$, ∇ and $\Delta^{(4)}$ are covariant lattice derivatives, $\tilde{\mathbf{E}}$ and $\tilde{\mathbf{B}}$ are improved chromo-electric and magnetic field strengths, n is a stability parameter that will be described below, and am_0 is the bare *b*-quark mass in lattice units. The c_i are the Wilson coefficients of the effective theory, and the terms are normalized such that they have the expansion $c_i = 1 + \alpha_s c_i^{(1)} + \mathcal{O}(\alpha_s^2)$. All gauge fields are tadpole improved with the fourth root of the plaquette $u_{0,P}$.

The one-loop corrections $c_i^{(1)}$ are described in [17], and we include these for c_1, c_4, c_5, c_6 in the high-β simulation and the nonperturbative determination of E_{sim}. The $c_i^{(1)}$ are functions of the effective theory cutoff, in this case, the bare quark mass am_0, but the total coefficient will also depend on the scale for α_s. We estimate the appropriate scale for several of the coefficients using the Brodsky-Lepage-Mackenzie (BLM) procedure [22], which gives $q^* = 1.8/a$ for c_1, c_6 and $q^* = 1.4/a$ for c_5. For c_4 we take $q^* = \pi/a$. The values of the one-loop corrections for two bare masses relevant to this calculation are given in Table I. We use α_s in the *V* scheme.

The *b*-quark propagators are generated by time evolution using the equation

$$G(\boldsymbol{x}, t+1) = \left(1 - \frac{a\delta H}{2}\right)\left(1 - \frac{aH_0}{2n}\right)^n U_t^\dagger(\boldsymbol{x})$$
$$\times \left(1 - \frac{aH_0}{2n}\right)^n \left(1 - \frac{a\delta H}{2}\right)G(\boldsymbol{x}, t) \quad (12)$$

for some initial condition $G(\boldsymbol{x}, 0)$. The parameter n is included for numerical stability and is set to 4, which is sufficient for all quark masses used here. Once it is high enough, results do not depend on the value of n [8].

The gluon action is a Symanzik-improved Lüscher-Weisz action [23,24],

$$S_{\text{LW}}[U] = \beta_{pl}\sum_x \frac{1}{N_c}\,\text{Re}\,\text{Tr}(\mathbb{1} - U_{pl})$$
$$+ \beta_{rt}\sum_x \frac{1}{N_c}\,\text{Re}\,\text{Tr}(\mathbb{1} - U_{rt})$$
$$+ \beta_{pg}\sum_x \frac{1}{N_c}\,\text{Re}\,\text{Tr}(\mathbb{1} - U_{pg}), \quad (13)$$

TABLE I. Values of the one-loop corrections in the series $c_i = 1.0 + \alpha_s c_i^{(1)}$ at two bare masses, and the scale at which each coefficient is evaluated.

Coefficient	$c_i^{(1)}$ $am_0 = 2.5$	$c_i^{(1)}$ $am_0 = 1.72$	q^*
c_1	0.95	0.766	$1.8/a$
c_4	0.78	0.691	π/a
c_5	0.41	0.392	$1.4/a$
c_6	0.95	0.766	$1.8/a$

where

$$\beta_{pl} = \frac{10}{g^2}, \quad (14)$$

$$\beta_{rt} = -\frac{\beta_{pl}}{20u_{0,P}^2}(1 + 0.4805\alpha_s), \quad (15)$$

$$\beta_{pg} = -\frac{\beta_{pl}}{u_{0,P}^2}0.03325\alpha_s. \quad (16)$$

$u_{0,P}$ is the tadpole improvement factor coming from the fourth root of the plaquette. The same action is used for the MILC gauge configurations used in the nonperturbative determination of E_{sim} and for the high-β simulations. The action in the high-β simulations includes an additional factor coming from the use of twisted boundary conditions; see Sec. III B. The value of α_s used in the improvement coefficients is given by the formula used by the MILC Collaboration [25]:

$$\alpha_s = 1.3036\log\left(u_{0,P}(\beta)\right). \quad (17)$$

Here we use the quenched values of $u_{0,P}(\beta)$ determined from our high-β configurations. The MILC configurations used in our nonperturbative analysis include sea quarks and thus have additional $O(n_f\alpha_s^2)$ contributions. However, these only affect E_0 at $O(n_f\alpha_s^3)$ and thus appear in terms we have not calculated anyway. These terms are part of our error budget. We give more details of the generation of high-β configurations in Appendix B.

Light sea quarks are included with the ASQtad-improved staggered action [26] in both the $n_f = 2 + 1$ MILC gauge configurations used to determine E_{sim} [25,27] and in the automated perturbation theory for E_0.

III. PERTURBATIVE DETERMINATION OF THE HEAVY QUARK ENERGY SHIFT

Here we first describe the calculation of the one-loop contribution and the two-loop fermionic contribution to E_0. The high-β method used to compute the gluonic two-loop contribution is described in the Sec. III B.

A. Automated lattice perturbation theory

We calculate the one-loop gluonic and the two-loop sea quark contributions to the heavy quark renormalization constants using the automated lattice perturbation theory routines HIPPY and HPSRC [28,29]. These routines have now been widely used and extensively tested in a variety of perturbative calculations, for example, in [10,17,30–35].

Evaluating the relevant Feynman integrals with HIPPY and HPSRC is a two-stage process: first, the PYTHON routine HIPPY generates Feynman rules encoded in "vertex files." These vertex files are then read in by the HPSRC code, a collection of FORTRAN modules that reconstruct the

diagrams and evaluate the corresponding integrals numerically, using the VEGAS algorithm [36]. All derivatives of the self-energy are implemented analytically using the derived TAYLOR type, defined as part of the TAYLUR package [37].

There are several advantages associated with using automated lattice perturbation theory, and the HIPPY/HPSRC routines in particular. First, automation removes the need to manipulate complicated expressions by hand. Second, the modular nature of the HIPPY and HPSRC routines greatly simplifies the use of different actions. Once Feynman diagrams are encoded in an HPSRC routine, the same calculation can be easily repeated with different quark and gluon actions by simply changing the input vertex files. This allows one to relatively easily reproduce previously published results for different actions, which serves as a nontrivial check of the routines.

Furthermore, the modules in HPSRC can be reused. We take advantage of this for the two-loop calculations presented in this paper: the same fermionic insertions in the gluon propagator appear in the two-loop diagrams for both the heavy quark energy shift and the tadpole improvement factor, u_0.

We wrote two "skeleton" one-loop HPSRC routines: one to calculate the one-loop energy shift and one for the one-loop tadpole improvement factor. Reproducing previously published results, such as those in [38,39], respectively, we confirmed that these one-loop routines were correct. The corresponding two-loop diagrams (see Fig. 1) are simply the one-loop skeleton diagrams with the "bare" gluon propagator replaced by the "dressed" gluon propagator that includes the fermion insertions; these insertions were calculated in a separate routine GLUON_SIGMA. This routine was debugged by confirming that the appropriate Ward identity was satisfied by the dressed gluon propagator.

At two loops there are four diagrams with internal fermions that contribute to the energy shift. We illustrate these contributions in Fig. 1. Double lines are heavy quark propagators coming from the improved NRQCD action, single lines are ASQtad sea quark propagators, and curly lines are from the Symanzik-improved gluon action. The radiative corrections to the NRQCD and ASQtad actions
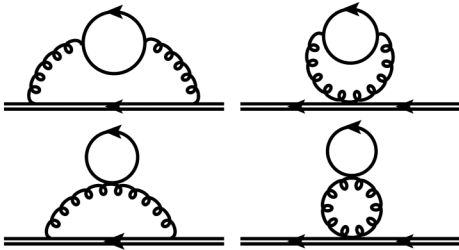
described in Sec. II C are not included in the perturbative calculation, as these only affect E_0 at higher orders in α_s.

We calculate the heavy quark energy shift at two different heavy quark masses, discussed in Sec. IV. At each heavy quark mass we use nine different light quark masses and extrapolate to zero light quark mass. We tabulate our extrapolated results in Table V (see Sec. V), where they appear as the n_f-dependent contribution to $E_0^{(2)}$.

The energy shift is infrared finite, but we introduce a gluon mass as an intermediate regulator to ensure convergence for the numerical integration. We confirm that the results are independent of the gluon mass for sufficiently small gluon mass, which in this case was approximately $a^2\lambda^2 < 10^{-6}$.

We will also need the sea quark contribution to the tadpole improvement factor u_0 since the high-β simulation includes only the gluonic piece. We calculate this using the automated perturbation theory. The perturbative expansion for the tadpole factor is written as

$$u_0 = 1 - u_0^{(1)}\alpha_L - u_0^{(2)}\alpha_L^2 + \mathcal{O}(\alpha_L^3). \quad (18)$$

The two-loop expansion for the plaquette tadpole is given by Mason [41], and we explicitly computed the one-loop coefficient and the two-loop n_f coefficient, which we quote here and which both agree with Mason's work. The result is

$$u_{0,P} = 1 - 0.76708(2)\alpha_L - (1.7723 - 0.069715(7)n_f)\alpha_L^2$$
$$+ \mathcal{O}(\alpha_L^3). \quad (19)$$

We require only the coefficient of $n_f\alpha_L^2$. For completeness, we also compute the two-loop n_f contribution to the Landau tadpole. The quenched two-loop Landau tadpole was computed by Nobes *et al.* [39] and, together with our result, the Landau tadpole is

$$u_{0,L} = 1 - 0.7501(1)\alpha_L - (2.06(1) - 0.0727(1)n_f)\alpha_L^2$$
$$+ \mathcal{O}(\alpha_L^3). \quad (20)$$

B. The high-β method

The high-β method allows us to compute the gluonic contributions to the quark propagator by generating an ensemble of quenched lattice gauge configurations at very weak coupling and calculating the dressed b-quark propagator. The energy of the propagator can then be described very well by a power series in the QCD coupling, which we fit to the Monte Carlo data to extract the relevant two-loop and higher contributions to E_0.

It is important in high-β studies to eliminate nonperturbative contributions that are due to the tunneling of fields and their associated Polyakov lines, or torelons, between Z_3 vacua associated with toron gauge configurations [42]. Such tunneling is suppressed using twisted boundary conditions [43–45] for which there is no zero mode for the non-Abelian gauge field. The Polyakov line that traverses

FIG. 1. Fermionic contributions to E_0, calculated using automated lattice perturbation theory. Double lines indicate heavy quarks, curly lines are gluons, and single lines represent light sea quarks.

all the directions with twisted boundary conditions has a nonzero expectation value for a given configuration. This expectation value is complex and, if no tunneling has occurred, it is proportional to an element of Z_3. We verify that this is the case for the configurations we use. As is shown later in this section [see the discussion leading to Eqs. (43) and (44)], twisted boundary conditions also considerably reduce finite-size, L-dependent effects, which significantly aids the fitting process.

We carry out the high-β simulation on finite-size lattices of volume $L^3 \times T$, with typically $T = 3L$, for a range of values for β and L. Here L is the spatial extent and T the temporal extent of the lattice. We use L values from 3 to 10 inclusive and β_{pl} values of 12, 15, 16, 20, 24, 27, 32, 38, 46, 54, 62, 70, 80, 92, and 120. We then perform a simultaneous fit in α_s and L to deduce the $L \rightarrow \infty$ limit for the expansion of measured quantities as a power series in α_s.

We denote the gauge fields by $U_\mu(x)$, and on a lattice with L_μ sites in the μ direction, they satisfy the boundary condition

$$U_\mu(x + L_\nu \boldsymbol{e}_\nu) = \Omega_\nu U_\mu(x) \Omega_\nu^\dagger, \quad (21)$$

where the twist matrices are defined by

$$\Omega_\mu \Omega_\nu = z^{n_{\mu\nu}} \Omega_\nu \Omega_\mu, \qquad z = \exp(2\pi i / N_c),$$
$$n_{\mu\nu} \in (0, \ldots, N_c - 1). \quad (22)$$

Here $n_{\mu\nu}$ is antisymmetric and its values must be chosen so that $\epsilon_{\mu\nu\sigma\rho} n_{\mu\nu} n_{\sigma\rho} = 0|_{N_c}$. This choice ensures that configurations have zero topological charge. For $N_c = 3$ we apply a nontrivial twist in the spatial directions, which we label 1, 2, and 3, with $n_{12} = n_{13} = n_{23} = 1$ and $n_{\mu 4} = 0$.

With twisted boundary conditions, the fermion fields ψ are $N_c \times N_c$ color-times-smell matrices. "Smell" is a new quantum number that allows twisted boundary conditions to be applied to fermion fields; color labels the rows and smell the columns. Then, as for the gauge fields,

$$\psi(x + L_\nu \boldsymbol{e}_\nu) = \Omega_\nu \psi(x) \Omega_\nu^\dagger. \quad (23)$$

Under a gauge transformation given by the $SU(N_c)$ field $g(x)$ the quantum fields transform as

$$U_\mu(x) \rightarrow g(x) U_\mu(x) g^\dagger(x + \boldsymbol{e}_\mu), \qquad \psi(x) \rightarrow g(x) \psi(x), \quad (24)$$

where $g(x + L_\nu \boldsymbol{e}_\nu) = \Omega_\nu g(x) \Omega_\nu^\dagger$. We define the auxiliary gauge fields

$$\tilde{U}_\mu(x) = \begin{cases} U_\mu(x) & x_\mu \neq L_\mu, \\ U_\mu(x) \Omega_\mu & x_\mu = L_\mu. \end{cases} \quad (25)$$

Then, under a gauge transformation, $\tilde{U}_\mu(x)$ transforms as in Eq. (24) but now with $g(x)$ regarded as periodic: $g(x + L_\mu \boldsymbol{e}_\mu) = g(x)$.

The gauge action is of the form

$$S(U) = \beta \sum_{P; x \in \Lambda} c_P f_P(x) P(\tilde{U}, x), \quad (26)$$

where Λ is the set of all lattice sites; $P(\tilde{U}, x)$ is the trace over a general Wilson loop; c_P is a numerical coefficient; and $f_P(x) \in Z_{N_c}$ is a phase factor defined by

$$f_P(x) = \prod_{\mu < \nu} (z^{n_{\mu\nu}})^{-\omega_{\mu\nu}(P,x)}. \quad (27)$$

Here $\omega_{\mu\nu}(P, x)$ is the winding number of the Wilson loop projected onto the (μ, ν) plane about the point $x_\mu = x_\nu = (L + 1/2)$. An explicit representation for the twist matrices Ω_μ is not needed to compute $f_P(x)$. When fermions are included, however, the implementation of twisted boundary conditions for general Wilson lines does require a representation for the Ω_μ to be chosen.

One method for implementing the boundary conditions extends the lattice by tiling with twisted periodic translations of the original configuration, effectively surrounding the lattice with a halo of links. This method has major disadvantages: it is difficult to parallelize because the physical sites are a subset of the tiled lattice array; it requires more storage; and in improved NRQCD the Wilson lines can extend far into the tiled region, which means that the extent of the halo needs to be significant. Rather than extending the lattice we write the action in terms of the auxiliary gauge fields, $\tilde{U}_\mu(x)$. Then one can show that all Wilson lines can be constructed using the auxiliary gauge fields with periodic boundary conditions multiplied on the right by an $SU(N_c)$ matrix. This $SU(N_c)$ matrix, which we denote $R(\mathcal{P})$, is constructed from a product of the twist matrices Ω_μ and is determined by the ordered and signed sequence in which the line crosses the boundaries. We now discuss this construction in more detail.

A general path $\mathcal{P}(x, y; \boldsymbol{s})$ starting at site x on a lattice in dimension D is defined by an ordered list $\boldsymbol{s} = [s_0, s_1, \ldots s_{l-1}]$ of signed integers, s_i, $1 \leq |s_i| \leq D$, which denote the steps along the path. The jth point on the path is z_j, where

$$z_0 = x, \qquad z_{j+1} = z_j + \boldsymbol{e}_{s_j}, \qquad 0 \leq j < l, \quad (28)$$

with the endpoint defined by $y = z_l$. We define the ordered product of links along the path $\mathcal{P}(x, y; \boldsymbol{s})$ as

$$\mathcal{L}(\tilde{U}; \mathcal{P}) = \left[\mathcal{T} \prod_{i=0}^{l-1} \tilde{U}_{s_i}(z_i) \right], \quad (29)$$

where, for $\mu \in \{1, 2, \ldots, D\}$,

$$\tilde{U}_{-\mu}(x) = \tilde{U}_\mu^\dagger(x - \boldsymbol{e}_\mu), \qquad \boldsymbol{e}_{-\mu} = -\boldsymbol{e}_\mu, \quad (30)$$

and the $\tilde{U}$ fields satisfy the periodic boundary condition

$$\tilde{U}_\mu(x + L_\nu \boldsymbol{e}_\nu) = \tilde{U}_\mu(x). \quad (31)$$

The ordering operator $\mathcal{T}$ means that matrices in the product are ordered from left to right with increasing index i. The Wilson line $L(\tilde{U}; \mathcal{P})$ associated with the path $\mathcal{P}(x, y; s)$ is then

$$L(\tilde{U}; \mathcal{P}) = \mathcal{L}(\tilde{U}; \mathcal{P})R(\mathcal{P}). \qquad (32)$$

To implement the twisted boundary conditions without using a lattice halo, we define the $SU(N_c)$ matrix as follows. A list $[c_0(x), c_1(x), \ldots, c_{p-1}(x)]$ is associated with the Wilson line starting at x, where the c_j are signed integers $1 \leq |c_j| \leq D$. The line crosses a boundary of the hypercube p times. On the jth crossing it crosses a boundary in a direction parallel to the μ_j axis in the positive (negative) direction. We define the corresponding c_j to be $c_j = -\mu_j(\mu_j)$. $R(\mathcal{P})$ is then given by

$$R(\mathcal{P}) = \left(\mathcal{T} \prod_{j=0}^{p-1} \Omega_{c_j} \right)^{\dagger}, \qquad (33)$$

with the convention $\Omega_{-\mu} = \Omega_{\mu}^{\dagger}$ and where $\mathcal{T}$ is the index-ordering operator defined above. $L(\tilde{U}; \mathcal{P})$ is then the parallel transporter from the endpoint y back to the starting point x. By expressing the Wilson line in terms of the $\tilde{U}$ fields, the boundary conditions are implemented simply by right-multiplication by $R(\mathcal{P})$. A similar result holds for the evolution of the NRQCD Green function, as we will describe below. With these conventions, a Wilson loop $W(x, s)$, located at x and defined by the path $\mathcal{P}(x, x; s)$, is given by

$$W(x, s) = \frac{1}{N_c} \text{Tr}(L(\tilde{U}; \mathcal{P}(x, x; s))). \qquad (34)$$

The basis states for the fermion field ψ are the N_c^2-independent $N_c \times N_c$, color-times-smell, real matrices. Twisted boundary conditions admit fractional momenta on the lattice, and for twisted boundary conditions in the 1, 2, 3 directions and periodic boundary conditions in the fourth direction, the allowed momenta are of the form

$$\begin{aligned} \boldsymbol{p} &= \frac{2\pi}{N_c L}(n_1, n_2, n_3, 0) + \boldsymbol{k}, \\ \boldsymbol{k} &= \left(\frac{\pi l_1}{L}, \frac{\pi l_2}{L}, \frac{\pi l_3}{L}, \frac{\pi l_4}{T} \right), \end{aligned} \qquad (35)$$

where the l_r, for $r = 1, 2, 3$, are integers with $-L/2 < l_r \leq L/2$ and $-T/2 < l_4 \leq T/2$ (with L and T assumed to be even). The possible entries in the integer vector $\boldsymbol{n} = (n_1, n_2, n_3, n_4)$ depend on the number of directions in which the boundary condition is twisted. In our case we have $0 \leq n_1, n_2 < N_c$, $n_3 = -(n_1 + n_2)|_{N_c}$ and $n_4 = 0$.

In NRQCD the source on the initial time slice for a Green function with momentum $\boldsymbol{p}$ is

$$\chi(\boldsymbol{p}, \boldsymbol{x}) = \frac{1}{L^3 N_c} \Gamma_{\boldsymbol{n}} e^{i\boldsymbol{p}\cdot\boldsymbol{x}}, \qquad (36)$$

$$\Gamma_{\boldsymbol{n}} = z^{\frac{1}{2}(n_1+n_2)(n_1+n_2-1)} \Omega_1^{-n_2} \Omega_2^{n_1}.$$

We need an explicit representation for the Ω_μ, where $\mu = 1, 2, 3$, and for $N_c = 3$ we choose

$$\Omega_1 = \begin{pmatrix} z & 0 & 0 \\ 0 & 1 & 0 \\ 0 & 0 & z^* \end{pmatrix} \qquad \Omega_2 = \begin{pmatrix} 0 & 1 & 0 \\ 0 & 0 & 1 \\ 1 & 0 & 0 \end{pmatrix} \qquad (37)$$

$$\Omega_3 = \Omega_1^{\dagger}\Omega_2^{\dagger}.$$

In the case of purely periodic boundary conditions we can take the source for the NRQCD Green function to be $\mathbb{1} \cdot e^{i\boldsymbol{p}\cdot\boldsymbol{x}}$, where $\mathbb{1}$ is the $N_c \times N_c$ unit matrix. This evolves all quark color states in one go. The analogous approach for quarks labeled by color times smell is not convenient, and so we evolve a source appropriately chosen from the basis of $N_c \times N_c$ matrices described above; color and smell singlet states, if needed, must then be constructed explicitly. The Green function $G(\boldsymbol{x}, \boldsymbol{p}, t)$ satisfies the usual twisted boundary conditions

$$G(\boldsymbol{x} + Le_\nu, \boldsymbol{p}, t) = \Omega_\nu G(\boldsymbol{x}, \boldsymbol{p}, t)\Omega_\nu^{\dagger}. \qquad (38)$$

The NRQCD evolution for $G(\boldsymbol{x}, \boldsymbol{p}, t)$ is given by the full NRQCD action and takes the form

$$G(\boldsymbol{x}, \boldsymbol{p}, t + 1) = \sum_{\boldsymbol{y}} K(\boldsymbol{x}, \boldsymbol{y}, t)G(\boldsymbol{y}, \boldsymbol{p}, t). \qquad (39)$$

The kernel K is given by

$$\begin{aligned} K(\boldsymbol{x}, \boldsymbol{y}, t) &= \left(1 - \frac{\delta H}{2} \right)\left(1 - \frac{H_0}{2n} \right)^n U_4^{\dagger} \\ &\times \left(1 - \frac{H_0}{2n} \right)^n \left(1 - \frac{\delta H}{2} \right), \end{aligned} \qquad (40)$$

with H_0, δH defined in Sec. II C.

We implement the operators in K using a PYTHON preprocessing package that defines each operator in H_0 and δH as a list of Wilson paths. The Wilson paths are each defined by a list $\boldsymbol{s}$ with a complex amplitude; these operator definitions are read in at run time. We apply the action of each operator on $G(\boldsymbol{y}, \boldsymbol{p}, t)$ with a standard function that first constructs the parallel transporter $L(\tilde{U}; \mathcal{P}(x, ys))$ for each path weighted by the associated amplitude, where $x = (\boldsymbol{x}, t + 1)$, $y = (\boldsymbol{y}, t)$, then performs the parallel transport of G from the tth to the $(t + 1)$th time slice, and finally accumulates the results in $G(\boldsymbol{x}, \boldsymbol{p}, t + 1)$. We solve the problem of implementing the twisted boundary conditions in carrying out this calculation by using $\tilde{U}$ fields. The net result is that the evolution equation can be written as

$$G(\boldsymbol{x}, \boldsymbol{p}, t + 1) = \sum_m b_m\left(\sum_{\boldsymbol{y}} \mathcal{L}(\tilde{U}; \mathcal{P}_m) \times G(\boldsymbol{y}, \boldsymbol{p}, t)R(\mathcal{P}_m) \right), \qquad (41)$$

where $\mathcal{P}_m = \mathcal{P}(x, y, s)m$ and the sum over m runs over all lists sm that define the kernel $K(x, y, t)$, with b_m the amplitude of the mth line. The matrix $R(\mathcal{P}_m)$ implements the twisted boundary conditions and is simple to compute for each $\mathcal{P}_m$. Because R right-multiplies the Green's function and time evolution is a left-multiplying operation, we can perform the time evolution for a given m using periodic boundary conditions for the $\tilde{U}$ fields and then independently right-multiply by the associated R matrix. This method removes the need for any halo of gauge fields, and the whole calculation can be easily parallelized.

Furthermore, twisted boundary conditions reduce finite-size effects in color singlet observables. To illustrate this result, we can consider the example of the correlator for a meson at rest, which is given by

$$M(t) = \sum_{y, \alpha} \text{Tr}[G_\alpha(y, 0; t) G_\alpha^\dagger(y, 0; t)], \qquad (42)$$

where α labels the basis matrix used for the source of the quark propagator located at the origin; all irrelevant spin degrees of freedom have been suppressed. The correlator $M(t)$ is the sum of weighted Wilson loops consisting of a Wilson line L_1, connecting $x = (0, 0)$ to $y = (y, t)$, followed by L_2 connecting y back to x and defined by the paths $\mathcal{P}_1 = \mathcal{P}(x, y, s_1)$ and $\mathcal{P}_2 = \mathcal{P}(y, x, s_2)$, respectively. Then $M(t)$ is of the form

$$M(t) = \sum_{\mathcal{P}_1, \mathcal{P}_2, y, \alpha} f(\mathcal{P}_1, \mathcal{P}_2) \text{Tr}[\mathcal{L}_1 \chi_\alpha R_1 R_2 \chi_\alpha^\dagger \mathcal{L}_2], \quad (43)$$

where $f(\mathcal{P}_1, \mathcal{P}_2)$ is the amplitude associated with the loop, $(\mathcal{P}_1 + \mathcal{P}_2)$, $\mathcal{L}_i = \mathcal{L}(\tilde{U}; \mathcal{P}_i)$ and $R_i = R(\mathcal{P}_i)$, for $i = 1, 2$. Irrespective of the details of $\mathcal{L}_1$ and $\mathcal{L}_2$, the term sandwiched in the middle is

$$\sum_\alpha \chi_\alpha R_1 R_2 \chi_\alpha^\dagger = \text{Tr}[R_1 R_2] \mathbb{1}. \qquad (44)$$

Since $R_1 R_2$ is a product of the Ω matrices and their conjugates, the trace in the above formula vanishes unless $R_1 R_2 = \mathbb{1}$. Thus, for a nonzero contribution, the Wilson loop composed of $\mathcal{P}_1$ and $\mathcal{P}_2$ must loop around the spatial torus a multiple of N_c times in such a way that $R_1 R_2 = \mathbb{1}$. This reduces finite-size effects, as the effective size of the lattice is now of order N_c times its spatial extent.

1. Perturbative fitting of E_0

We obtain the quark propagator by averaging $G(x, p, t)$ over the ensemble of high-β configurations. Because $G(x, p, t)$ is not gauge invariant we fix the configurations to Coulomb gauge. We then define the Coulomb ensemble-averaged quark propagator by

$$\hat{G}(p, t, \beta, L) = \left\langle \sum_x \text{Re Tr}(\Gamma_n^\dagger e^{-ip \cdot x} G(x, p, t)) \right\rangle_{L, \beta}. \qquad (45)$$

Here we write $\hat{G}(p, t, \beta, L)$ as a function of L to indicate explicitly that there are finite-size effects, which must be accounted for to extract the desired $L \to \infty$ result.

In order to extract the two-loop and three-loop coefficients in the perturbation expansion for E_0 using the high-β method, it is necessary to carry out a simultaneous two-parameter fit in α_s and L. The fit is a power series in α_s and in $1/L$, and we measure the $L \to \infty$ coefficient of the α_s^n, for $n = 2, 3$, terms. Because the signal for the two-loop, α_s^2, term is small compared with the one-loop contribution, the accuracy of the fit is greatly improved by calculating the one-loop coefficient analytically, thus determining the coefficient of α_s in the fit. However, Feynman perturbation theory on the lattice gives the result for lattices of large temporal extent, $T \to \infty$, while here we need to carry out the perturbation theory for varying finite $T = 3L$. We describe the finite volume perturbation theory for the NRQCD evolution equation in Appendix A. It turns out that a minor modification of the rules for automated Feynman perturbation theory accounts for the effects of finite T in the one-loop case.

For large enough t, we have that

$$\hat{G}(p, t, \beta, L) = Z_\psi e^{(E_0 + \mathbf{p}^2/2M_{\text{pole}} + \cdots)t}, \qquad (46)$$

and by fitting to this form for a range of values of p, we can, in principle, extract the renormalization constants Z_ψ, Z_{m_0} and E_0. However, for the current work we do not need Z_{m_0}, as we extract M_{pole} using Eq. (1) rather than Eq. (3) since, as remarked in Sec. II A, the statistics available are not sufficient to extract a reliable value for Z_{m_0}. We therefore evaluate $\hat{G}$ for $p = 0$ and measure $E_0(\beta, L)$, the energy as a function of β and L.

From the boundary condition we have $\hat{G}(p, t = 0, \beta, L) = 1$, and so we cannot fit to the asymptotic form below some value $t = t_{\text{min}}$. It is a feature of Coulomb gauge that Z_ψ is very close to unity. This is borne out by our one-loop perturbation theory and also by simulation. Consequently, considering Z_ψ and E_0 as functions of t, we expect the t dependence of Z_ψ to be small compared with that of E_0 and that t_{min} is not too large. While accounting for the need to measure in the asymptotic region by fitting only for $t \geq t_{\text{min}}$, it is useful to account for any residual t dependence by including a transient function of t in the exponent in Eq. (46). From the finite volume perturbation theory and from Eqs. (A11) and (A12), $E_0^{(1)}(L, T, t)$ and $Z_\psi^{(1)}(L, T, t)$ depend on t, and a fit to their t dependence for small t gives a good indication of the explicit transient function we should choose. Using the one-loop calculation in this way, we find that to extract $E_0(\beta, L)$ from the high-β simulation, the form for $\hat{G}$ should be chosen as

$$\hat{G}(0, t, \beta, L) = Z_\psi(\beta, L) e^{(E_0(\beta, L)t + C/t)}, \quad t \geq t_{\text{min}}, \qquad (47)$$

where, in practice, we choose $t_{\text{min}} = 5$ for all L.

We fit $E_0(\beta_{pl}, L)$ to a joint power series in $\alpha_V^{(n_f)}(q^*)$ and $1/L$, with $n_f = 3$. In order to do this we need to compute the value of $\alpha_V^{(3)}(q^*)$ given the value of β_{pl} with which the quenched configurations were generated. We first compute $\alpha_V^{(0)}(q^*)$ from the measured plaquette using perturbation theory. The lattice coupling α_L, deduced directly from the value of β_{pl}, can be expressed as a perturbation series in $\alpha_V^{(n_f)}(q^*)$ for any n_f. We eliminate α_L by equating the series for $n_f = 0$ with that for $n_f = 3$ and thus deduce a power series for $\alpha_V^{(3)}(q^*)$ expanded in powers of $\alpha_V^{(0)}(q^*)$. In this way we compute the required value of $\alpha_V^{(3)}(q^*)$ for each value of β_{pl}. The details follow.

We choose the V scheme defined in terms of the color Coulomb potential, and the value of q^* is found by using the BLM procedure [22,46] applied to the heavy quark self-energy for determining E_0; Müller [40] gives $q^* = 0.794a^{-1}$ for this case. To determine $\alpha_V^{(3)}(q^*)$ given β we use the value of the Wilson plaquette, $W_{11}(\beta)$, from our configurations to calculate $\alpha_V^{(0)}(q^*)$ using the perturbative expansion of W_{11}. The BLM procedure gives the optimal value of $q^* = 3.33a^{-1}$ for this quantity [41,47,48]. Note that we compute $\alpha_V^{(0)}(q^*)$ in this manner, i.e. for $n_f = 0$, since we are using quenched configurations. Then we have $(n_f = 0)$

$$\log(W_{11}) = -3.068\alpha_V^{(0)}(q^*)(1 - 0.5945(2)\alpha_V^{(0)}(q^*)$$
$$- 0.589(38)\alpha_V^{(0)}(q^*)^2 + \cdots). \quad (48)$$

We do not find any dependence of W_{11} on L since it is a short-distance, UV, quantity. We now relate $\alpha_V^{(0)}(q^*)$ to $\alpha_L(a)$ using [41,49]

$$\alpha_L(a) = \alpha_V^{(n_f)}(q)(1 - v_1^{(n_f)}(q)\alpha_V^{(n_f)}(q)$$
$$- v_2^{(n_f)}(q)\alpha_V^{(n_f)}(q)^2),$$

$$v_1^{(n_f)}(q) = 2\beta_0 \log(\pi/q) + 3.57123 - 0.001196n_f,$$

$$v_2^{(n_f)}(q) = 2\beta_1 \log(\pi/q) - [v_1^{(n_f)}]^2 + 5.382 - 1.0511n_f,$$

where β_0 and β_1 are the coefficients in the β function,

$$\beta_0 = \frac{1}{4\pi}\left(11 - \frac{2}{3}n_f\right), \qquad \beta_1 = \frac{1}{(4\pi)^2}\left(102 - \frac{38}{3}n_f\right),$$
$$(49)$$

and then we use this expansion to reexpress the result in terms of $\alpha_V^{(n_f)}(q^*)$. We find

$$\alpha_V^{(n_f)}(q) = \alpha_V^{(0)}(q)(1 + u_1(q)\alpha_V^{(0)}(q) + u_2(q)\alpha_V^{(0)}(q)^2),$$

$$u_1(q) = v_1^{(n_f)}(q) - v_1^{(0)}(q),$$

$$u_2(q) = v_2^{(n_f)}(q) - v_2^{(0)}(q) + u_1(q)v_1^{(n_f)}(q).$$

We then run $\alpha_V(q^*)$ from $q^* = 3.33a^{-1}$ to $q^* = 0.794a^{-1}$, appropriate for the fit to $E_0(\beta, L)$, using the three-loop running

$$\frac{d\alpha_V(\mu)}{d\log\mu^2} = -\alpha_V(\mu)^2(\beta_0 + \beta_1\alpha_V(\mu) + \beta_{2V}\alpha_V(\mu)^2),$$

$$\beta_{2V} = \frac{1}{(4\pi)^3}(4224.18 - 746.006n_f + 20.8719n_f^2),$$

where we suppress the n_f superscript from now on, using $n_f = 3$ implicitly.

We fit $\hat{G}(0, t, \beta, L)$ separately, as discussed above, for the set of β, L values and deduce $E_0(\beta, L)$. As the data may contain residual autocorrelations, we resample via blocking to determine the true statistical error. Within independent chains, sequential measurements are grouped together into bins, and the means of each bin are treated as statistically independent. The size of the bins is determined by examining the scaling of the variance as a function of the bin size, and is dependent on the values of L and β_{pl}, and the operator being measured. We then fit these values to the form

$$E_0(\beta, L) = (E_0^{(1)}(L, T/2) + \delta)\alpha_V(q^*)$$
$$+ \left(c_{20} + \frac{1}{L}c_{21}\right)\alpha_V(q^*)^2 + c_{30}\alpha_V(q^*)^3, \quad (50)$$

with $q^* = 0.794a^{-1}$ and $T = 3L$. Here $E_0^{(1)}(L, T/2)$ is the calculated value for the one-loop contribution which includes the contribution from tadpole improvement of the
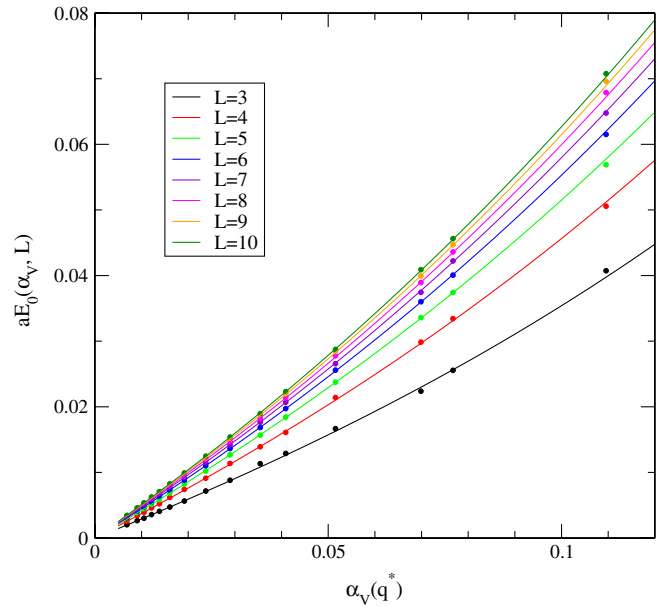

FIG. 2 (color online). $E_0(\alpha_V(q^*), L)$ for $aM = 1.72$ for both data and the fit for the values of lattice size $L^3 \times T$, $T = 3L$ used in the extraction of the two- and three-loop quenched coefficients in the perturbation series for E_0. We write E_0 as a function of the $\alpha_V(q^*)$ value rather than β_{pl}. Here $q^* = 0.794a^{-1}$. This fit has $\chi^2 = 1.2$.

NRQCD Hamiltonian; this contribution is a constant, independent of β and L. We allow for a small additive adjustment δ, independent of β_{pl} and L, in the values of the $E_0^{(1)}(L, T/2)$ accounting for any minor mismatch between their analytical and numerical calculations; as we should expect, δ is found to be very small. The finite-size, L, dependence of E_0 is included in $E_0^{(1)}(L, T/2)$ and in the two-loop coefficient. We find that this parametrization is sufficient for a very good fit to the data; within errors we do not discern any α^2/L^2 or α^3/L contributions. The fit is for 116 degrees of freedom (4 parameters, 15 β values and 8 L values), and we find $\chi^2 = 1.2$ and 1.1, respectively, for $am_0 = 1.72, 2.5$. In Fig. 2 we show $E_0(\beta, L)$ plotted versus $\alpha_V(q^*)$ for the different L and for $am_0 = 1.72$. The quenched results that we require are $E_0^{(2),q} = c_{20}$.

IV. NONPERTURBATIVE DETERMINATION OF $E_{\rm sim}$

We now briefly discuss the nonperturbative determination of the meson energies $E_{\rm sim}$. The method is standard, and this NRQCD action [17] has been thoroughly tested by HPQCD in a range of calculations.

We use two ensembles of gauge configurations generated by the MILC Collaboration with $n_f = 2 + 1$ ASQtad sea quarks, which we denote as coarse (~ 0.12 fm) and fine (~ 0.09 fm) [25,27]. Details are given in Table II. The light quark masses on these ensembles are not particularly chiral, but we have seen that the light sea quark mass has a negligible effect on most quantities in the bottomonium spectrum [17]. The lattice spacing on these ensembles has been determined using the static quark potential parameter r_1 in [50] and is given in the table.

The NRQCD action is given in Sec. II C and includes one-loop radiative corrections to the coefficients calculated in [17,51]. The coefficients are listed in Table III. The same coefficients are used in the perturbative calculations and in the high-β simulations, but with α_s evaluated at a scale appropriate for β, as discussed in Sec. II C.

Tuning the bare b-quark mass accurately is an important part of the calculation, as this is a potential source of error in $\bar{m}_b(\bar{m}_b)$. The heavy quark energy shift means that we cannot tune using the meson energy directly, but we must use the kinetic mass determined from the dispersion

TABLE III. Coefficients used in the nonperturbative simulation. $u_{0,P}$ is the plaquette tadpole improvement factor, and c_i are the coefficients in δH.

Set	$u_{0,P}$	c_1	c_2	c_3	c_4	c_5	c_6
Coarse	0.86879	1.31	1.0	1.0	1.2	1.16	1.31
Fine	0.878214	1.21	1.0	1.0	1.16	1.12	1.21

relation, which is much noisier. A detailed study of the systematic errors incurred and their effect on the accuracy of the bare mass was carried out in Ref. [17]. To reduce systematic errors we use the spin average of the vector and pseudoscalar bottomonium states,

$$\overline{M_{b\bar{b}}} = (3M_{{\rm kin},\Upsilon} + M_{{\rm kin},\eta_b})/4, \qquad (51)$$

which eliminates errors from missing spin-dependent higher-order terms and radiative corrections in the action. We must also take account of missing electromagnetic effects, sea charm quarks and annihilation of the η_b to gluons by shifting the experimental values appropriately. These effects were estimated in [20], resulting in an adjusted experimental value of $M_{b\bar{b}}^{\rm expt} = 9.450(4)$ GeV, where the error comes from taking a large uncertainty on the shifts that were applied. The correctly tuned bare b-quark masses in lattice units that we obtain are $2.49(2)_{\rm stat}(1)_{\rm sys}$ on the coarse lattice, and $1.71(2)_{\rm stat}(1)_{\rm sys}$ on the fine lattice. The first error includes a sizable statistical error from the kinetic mass and all lattice spacing errors; the second includes the systematic errors in the kinetic mass estimated in [17]. The effect of these errors is included in the final error budget.

The valence strange quark propagators used in the B_s mesons utilize the highly improved staggered quark (HISQ) action [52] and are tuned using the η_s meson. This is a fictitious $s\bar{s}$ particle which, with the addition of experimental data for M_π, M_K and chiral perturbation theory, is a very convenient choice for tuning the s mass and fixing the scale. The value on the $n_f = 2 + 1$ ensembles that we are using is $M_{\eta_s} = 0.6858(40)$ GeV [50].

The ground state energies $E_{\rm sim}$ are extracted from multiexponential Bayesian fits [53] to meson correlation functions that use multiple smeared sources for the quark propagators. To further improve statistics we use stochastic

TABLE II. Details of the two ASQtad gauge configurations used in the nonperturbative determination of $E_{\rm sim}$. β is the gauge coupling, a^{-1} is the inverse lattice spacing determined using the static quark potential parameter r_1, $u_0 am_l$, $u_0 am_s$ are the light sea quark masses, L and T are the lattice dimensions, and $n_{\rm cfg}$ is the size of the ensemble.

Set	β	a^{-1} (GeV)	$u_0 am_l$	$u_0 am_s$	$L \times T$	$n_{\rm cfg}$
Coarse	6.76	1.652(14)	0.01	0.05	20×64	1380
Fine	7.09	2.330(17)	0.0062	0.0310	28×96	904

TABLE IV. Masses and extracted energies from the nonperturbative simulations. am_0 and am_s are the bare (valence) b and s masses, and $aE_{{\rm sim},X}$ are the fitted ground state energies of the meson X in lattice units. The first row is for the coarse ensemble and the second for fine. The errors are from statistics and/or fitting only.

am_0	$am_s^{\rm val}$	$aE_{{\rm sim},\Upsilon}$	$aE_{{\rm sim},\eta_b}$	$aE_{{\rm sim},B_s}$	$aE_{{\rm sim},B_s^*}$
2.50	0.0496	0.46591(6)	0.42579(3)	0.6278(5)	0.6595(6)
1.72	0.0337	0.41385(4)	0.38124(2)	0.4812(5)	0.5027(7)

noise sources and run 16 time sources on each configuration for the Υ, and 4 for the B_s. The results are listed in Table IV.

V. CALCULATING THE $\overline{\text{MS}}$ *b*-QUARK MASS

Now that E_0 and E_{sim} have been determined, we can combine the results into a perturbative series for $\overline{m}_b(\overline{m}_b)$ in the $\overline{\text{MS}}$ scheme. This requires various scheme conversions and changes of scale to give the series at the scale relevant for the *b*-quark mass. This then gives the result at $n_f = 3$, and we can use known formulas to convert this to the usual $n_f = 5$ result. We repeat this whole process at both values of the bare mass to check for discretization errors which will then be included in our error.

To further reduce systematic errors, we adjust Eq. (1) so that we use the spin-averaged bottomonium mass $M_{b\bar{b}} = (3M_{\Upsilon} + M_{\eta_b})/4$. This removes any error from spin-dependent terms in the NRQCD action. As discussed in Sec. IV, the experimental result used must be adjusted to $M_{b\bar{b},\text{expmt}} = 9.450(4)$ GeV to reflect the absence of electromagnetism, sea charm quarks and η_b annihilation.

A. Perturbative series for $\overline{m}_b(\overline{m}_b)$

So far, all our perturbative results have been expressed in terms of α_V, the coupling constant defined in the *V* scheme at the scale $q^* = 0.794/a$.

$$aE_0 = aE_0^{(1)}\alpha_V(q^*) + (aE_0^{(2)} + aE_0^{u0,f})\alpha_V^2(q^*)$$
$$+ aE_0^{(3),q}\alpha_V^3(q^*). \quad (52)$$

The results for each component are given in Table V.

The series expansion of aE_0 is truncated at α_s^3, and we take $n_f = 3$, as this is the number of sea quarks in the nonperturbative determination of E_{sim}. No fermionic α_s^3 contributions are included in the series. The effects of the one-loop tadpole corrections are directly included in the tadpole-improved results from the high-β simulation, as are the quenched two-loop tadpoles. However, the two-loop fermionic tadpole contributions are not included in the high-β results so we must add the corresponding correction $aE_0^{u0,f}$ to the energy shift. $aE_0^{u0,f}$ is given by [38]

TABLE V. Perturbative results required to extract the $\overline{\text{MS}}$ mass. The quenched results, indicated by the superscript *q*, are from high-β simulations. The one-loop data are the exact perturbative results extrapolated to infinite lattice size. The two-loop results include both quenched and fermionic contributions. The three-loop values include only quenched results. We evaluate all results in the *V* scheme at a characteristic scale of $q^* = 0.794a^{-1}$ [40].

am_0	$aE_0^{(1)}$	$aE_0^{(2)}$	$aE_0^{u0,f}$	$aE_0^{(3),q}$
2.50	0.6786(1)	$1.16(4) - 0.2823(6)n_f$	$0.158531(16)n_f$	2.3(3)
1.72	0.5752(1)	$1.30(4) - 0.3041(3)n_f$	$0.186607(19)n_f$	2.3(3)

$$aE_0^{u0,f} = \left[1 + \frac{7}{2am_0} - \frac{3}{2}\left(\frac{1}{a^3m_0^3} + \frac{1}{2na^2m_0^2}\right)\right]u_0^{(2),f}, \quad (53)$$

where $u_0^{(2),f}$ is the fermionic contribution to $u_{0,P}$ given in Sec. III A.

The other perturbative factor that we need is the pole to $\overline{\text{MS}}$ renormalization Z_M, which is reproduced in Appendix C. Inserting these two series into Eq. (7) gives a series for $\overline{m}_b(\overline{m}_b)$.

We now relate $\alpha_V(q^*)$ to $\alpha_{\overline{\text{MS}}}(q^*)$. This is done using the three-loop relation in [54–56], which is summarized in Appendix C, and we express E_0 as a series in the $\overline{\text{MS}}$ scheme. Matching is done at q^* to avoid logarithmic contributions. The series is then run to $\mu = 4.2$ GeV using the four-loop $\overline{\text{MS}}$ beta function.

To evaluate the series we need the relevant value of $\alpha_{\overline{\text{MS}}}$, which in this case is the three-flavor value at $\bar{m}_b$. Since $\overline{\text{MS}}$ is a mass-independent scheme, high mass particles do not explicitly decouple from the beta function, and one must construct an effective theory with $n_l = n_f - 1$ quarks when crossing a quark mass threshold [57]. This introduces discontinuities in the running of $\alpha_{\overline{\text{MS}}}$ at the thresholds which have been calculated to four loops in [58], and we give the relevant formulas in Appendix C. We start with the current PDG average $\alpha_{\overline{\text{MS}}}(M_Z, n_f = 5) = 0.1184(7)$ which we run to 4.2 GeV using the four-loop running with $n_f = 5$ [59]; then we match to the $n_f = 4$ theory and run down to 1.2 GeV to match to $n_f = 3$, before running back up to 4.2 GeV with $n_f = 3$ running. We find $\alpha_{\overline{\text{MS}}}(\bar{m}_b, n_f = 3) = 0.2159(20)$. Small changes in the matching scales have a negligible effect on the value.

Using this value of the coupling, the results using $M_{\bar{b}b}$ are $\overline{m}_b(\overline{m}_b, n_f = 3) = 4.195(8)$ GeV on the coarse lattice and $\overline{m}_b(\overline{m}_b, n_f = 3) = 4.198(10)$ GeV on the fine lattice. We also tried allowing the scale to float and solving such that μ was exactly the $\overline{\text{MS}}$ mass, but this makes a negligible difference to the result. The results using the B_s mass give $\overline{m}_b(\overline{m}_b, n_f = 3) = 4.177(8)$ GeV on the coarse lattice and $\overline{m}_b(\overline{m}_b, n_f = 3) = 4.191(10)$ GeV on the fine lattice. These are consistent with the bottomonium results. This error includes statistical errors in the perturbation theory integrals, lattice spacing error, and simulation errors in the ground state masses (negligible). We have not yet included an estimate of the truncation error in the perturbative series.

Our calculations were performed using lattice results with $n_f = 3$ sea quarks. In order to compare to the real world we must match this value to $n_f = 5$. As with the coupling constant, a running quark mass in a mass-independent scheme is discontinuous at flavor thresholds and must be matched to an effective theory with a different number of flavors. The formula for the mass decoupling is given in Appendix C in Eq. (C12). We run down to 1.2 GeV

with three flavor mass running [59], match to a theory with $n_f = 4$, run up to 4.2 GeV and match to the $n_f = 5$ theory. Again, small changes to the matching scale or the final scale at which we evaluate the mass have a negligible effect. After this running, the values we obtain for the $M_{\bar{b}b}$ results are $\overline{m}_b(\overline{m}_b, n_f = 5) = 4.161(10)$ GeV on the coarse lattice and $\overline{m}_b(\overline{m}_b, n_f = 5) = 4.164(12)$ GeV on the fine lattice, where from now on we state n_f explicitly. Overall, matching to the $n_f = 5$ theory shifts the mass down by around 30 MeV.

In principle, there may be discretization errors arising from lattice artifacts. Since we have two lattice spacings available we can fit the results as a function of a to obtain the physical result and to allow a systematic error for this dependence. In fact, the dependence is very mild, as is clear from the fact that all of the results are consistent with each other. Our NRQCD action contains discretization corrections that get renormalized as a function of the cutoff am_0, and so we allow an additional mild dependence of the fit function on am_0. This makes no difference on the fit. The form is

$$\overline{m}_b(\overline{m}_b)(a, \delta x_m) = \overline{m}_b(\overline{m}_b) \times \left[1 + \sum_{j=1}^{2} d_j (\Lambda a)^{2j} \right.$$
$$\left. \times (1 + d_{jb}\delta x_m + d_{jbb}(\delta x_m)^2) \right], \quad (54)$$

where we have allowed discretization effects with a scale of $\Lambda = 0.5$ GeV and cutoff dependence via $\delta x_m = (am_0 - 2.1)/(2.5 - 1.7)$ which varies between ± 0.5. Priors on the values are 4.2(5) for the mass, 0.0(3) for the a^2 term (since our action is one-loop improved), and 0(1) for everything else.

Some of the errors in the data are correlated, and we allow for this in the fit. We multiply the $\bar{m}_b$ values by a $(1 + n_f \alpha_s^3)$ truncation error (discussed below) which is 100% correlated between the points on the two lattice spacings. The errors on all quantities coming from the high-β simulations are correlated with corresponding errors on the other lattice spacing. Statistical errors coming from VEGAS integrals are uncorrelated.

We only fit the bottomonium results, as the B_s results are in very good agreement. The fit is shown in Fig. 3 and gives $\overline{m}_b(\overline{m}_b, n_f = 5) = 4.166(42)$ GeV.

B. Error budget

Broadly, the three main sources of uncertainty in our result for the *b*-quark mass are statistical errors, errors from truncating the perturbation series, and other systematic errors. We expect the $\mathcal{O}(\alpha_s^3)$ perturbative contributions to dominate the uncertainty in our final result. In this section we discuss each of these sources of error in turn and tabulate our error budget in Table VI.
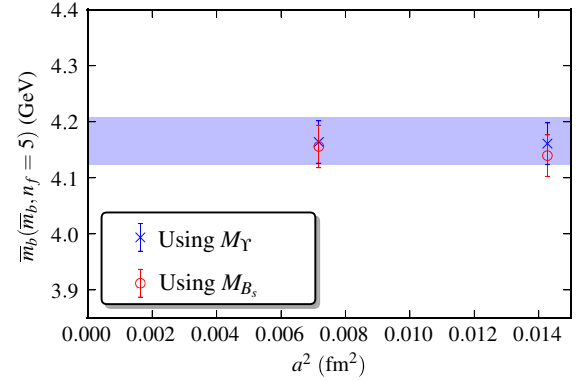

FIG. 3 (color online). Results for the $n_f = 5$ $\overline{\text{MS}}$ mass using both bottomonium and B_s meson simulation data, and the fit to the bottomonium results. The errors on the data points include statistics, error on $\alpha_{\overline{\text{MS}}}$ and a correlated truncation error on the perturbative series. Additional (subdominant) errors are described in the text.

(a) *Statistical errors.*—Statistical errors arise in the nonperturbative calculation of E_{sim} and in the contributions at each order in the expansion of the heavy quark energy shift E_0. The statistical error in E_{sim} comes from the fit to lattice two-point functions and is completely negligible. The statistical error in the one-loop piece of E_0 comes from the evaluation of diagrams using VEGAS and from the extrapolation to infinite volume. The uncertainties in the two-loop and three-loop quenched coefficients of E_0 arise from the simultaneous fit to α and L. This is significant at 14 MeV. The statistical error in the two-loop fermionic coefficient is due to the numerical evaluation of the Feynman diagrams and the extrapolation to zero light quark mass.

TABLE VI. The *b*-quark mass error budget. Systematic error estimates are discussed in more detail in the text.

Source	Error (MeV)	Error (%)
$n_f \alpha_s^3$ perturbative error	36	0.9
M_Υ, M_{η_b} experiment	<0.1	<0.01
aE_{sim}	<0.1	<0.01
am_0 tuning	6	0.14
VEGAS integration	<0.1	<0.01
High-β statistics	14	0.35
a dependence	16	0.38
Scale uncertainty	4.4	0.10
α_s uncertainty	0.2	0.01
Relativistic v^6	5	0.12
Radiative $\alpha_s v^4$	2.5	0.06
E&M, charm sea, annih.	1.9	0.05
Total	43 MeV	1.0%

(b) *Perturbative errors.*—The three-loop fermionic contribution to the energy shift is unknown, so we estimate the error due to this contribution as $\mathcal{O}(n_f \times \alpha_{\overline{\mathrm{MS}}}^3)$. This is the dominant source of error in our calculation. Perturbative errors from running the coupling and quark mass are negligible, as the formulas are higher order.

The fermionic contributions are the only unknown source of uncertainty at three loops in our result. In principle, these effects can be calculated using automated lattice perturbation theory. However, there are a large number of diagrams to evaluate, many of which are likely to have complicated pole structures and possible divergences (the energy shift is infrared finite, but individual diagrams may have divergences that ultimately cancel). The complexity of such a calculation would be considerable.

(c) *Other systematic errors*

   (i) Bare mass tuning: The tuning of the bare *b*-quark mass used in E_0 and E_{sim} is a source of error. We can estimate the error due to mistuning using the errors given on the tuned masses $2.49(2)_{\mathrm{stat}}(1)_{\mathrm{sys}}$ and $1.71(2)_{\mathrm{stat}}(1)_{\mathrm{sys}}$ and by estimating the bare mass dependence of each quantity. We use only the one-loop piece of E_0 and compute the value at an extra mass; we find a linear dependence with a slope of 0.13. For E_{sim} we use the results at different bare masses given in [17] and find a dependence that is less than 0.01, which we take to be linear for these small increments. By recomputing $\overline{m}_b(\overline{m}_b)$ taking a 1σ deviation in the bare mass, we find errors of 4 MeV on the coarse lattice and 6 MeV on the fine lattice. We take the larger of these as an error on our result.

   (ii) Corrections for missing electromagnetism, charm quarks in the sea and η_b annihilation were estimated and applied to the experimental Υ, η_b masses. We add the errors linearly rather than in quadrature and propagate this error through to the final result, which gives 1.9 MeV.

   (iii) Higher-order relativistic corrections: These arise from not including $\mathcal{O}(v^6)$ terms in our NRQCD action and, with $v^2 \sim 0.1$, could contribute 1% of the binding energy, which is 5 MeV.

   (iv) Radiative corrections: $\alpha_s^2 v^4$ should be smaller at around half a percent of the binding energy, so we take 2.5 MeV.

   (v) Lattice spacing errors, including r_1/a: These are included as the "statistical" error on the data points in the plot, but we estimate their contribution to the final error to be 4.5 MeV.

   (vi) Lattice spacing dependence: We incur an error from fitting the two masses as a function of a,

which we can estimate from the fit. The lattice spacing dependence is not significant, but we find 16 MeV; this is already included in the total error quoted from the fit.

   (vii) Sea quark mass dependence: We have only used one sea quark mass in our calculation, but in previous calculations we have observed very mild dependence in E_{sim} [17]. Errors from light sea quark mass dependence should be negligible compared to our other errors.

With these errors included, our final result for the $\overline{\mathrm{MS}}$ *b*-quark mass is

$$\overline{m}_b(\overline{m}_b, n_f = 5) = 4.166(43) \text{ GeV}. \tag{55}$$

VI. DISCUSSION

We can compare our result to previous values from the literature. As discussed in Sec. I, there are a number of accurate theory results from comparing continuum QCD perturbation (through α_s^3) for moments of the vector charmonium current-current correlator to experimental results extracted from $\sigma(e^+e^- \to \text{hadrons})$ in the *b* region. In [1], for example, the result $\overline{m}_b(\overline{m}_b) = 4.163(16)$ GeV is obtained. In [5] lattice QCD calculations of time moments of the η_b correlator are used instead of the experimental results to give $\overline{m}_b(\overline{m}_b) = 4.164(23)$ GeV. It is important in this calculation to use pseudoscalar correlators in a lattice QCD formalism (HISQ) that has absolutely normalized pseudoscalar currents. Our result agrees with these two values. It is not as accurate because we are not using such high-order QCD perturbation theory, but it nevertheless provides a check from a completely different perspective at the level of 1%.

There are also a number of results using alternative methods from lattice QCD, but these are not typically very accurate. An early result for $\overline{m}_b$ with NRQCD *b* quarks on the $n_f = 2 + 1$ MILC configurations including *u*, *d* and *s* sea quarks was 4.4(3) GeV [8], the large error here arising from the use of one-loop lattice QCD perturbation theory for Z_M. More recently, methods have been developed by the ALPHA Collaboration for determining the energy shift for lattice heavy quark effective theory nonperturbatively, including next-to-leading-order terms in the inverse heavy quark mass expansion for the valence *b* quarks [60]. This has been implemented on gluon field configurations including *u* and *d* sea quarks in the clover formalism. Combining with the experimental *B* meson mass in a similar approach to the one used here, we get $\overline{m}_b(\overline{m}_b) = 4.22(11)$ GeV. The error here is dominated by lattice statistical and systematic errors. Another method by the ETM Collaboration [61] uses a ratio of quark masses to heavy-light meson masses with a known infinite mass limit. This is implemented on gluon field configurations including *u* and *d* sea quarks in the twisted mass formalism and valence *b* and light twisted mass quarks. Interpolating
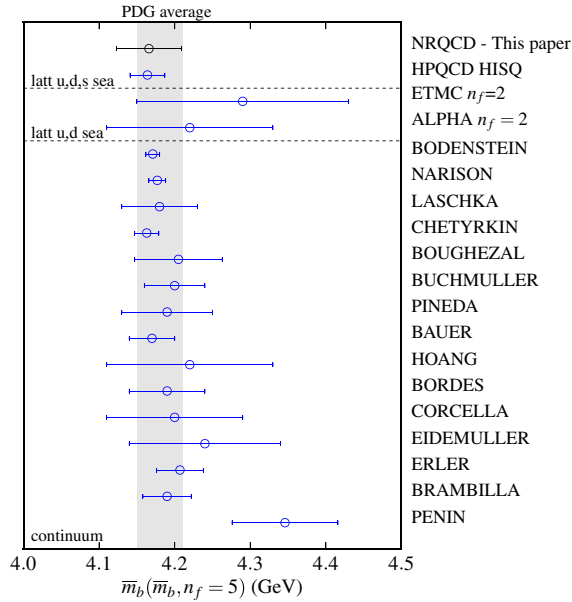
FIG. 4 (color online). Comparison of our result with other recent theory-based b-quark mass determinations. We include all determinations listed in the PDG summary table [62] but separate lattice QCD determinations with $n_f = 2$ and $n_f = 2 + 1$ sea quarks for easier comparison [1,2,5,60,61,67–79].

to the b quark and using experimental meson masses gives $\overline{m}_b(\overline{m}_b) = 4.29(14)$ GeV, with an error dominated by lattice statistical errors. Note that neither the ALPHA or ETM results include s quarks in the sea, and the error from this is not estimated.

Figure 4 collects a number of lattice and continuum QCD determinations of the b-quark mass for comparison. The evaluation of 4.18(3) GeV in the Particle Data Tables [62] is shown by the grey band. There is good consistency between all determinations, including the new result of this paper and results not yet included in the PDG average [80].

VII. CONCLUSION

In this paper we have presented a new determination of the b-quark mass from simulations of lattice NRQCD at two heavy quark masses. The uncertainty associated with previous determinations of the b-quark mass from lattice NRQCD was dominated by the one-loop perturbative calculations used to extract the b-quark mass. By calculating the heavy quark energy shift at two loops, we have significantly reduced this uncertainty. The resulting error is now in line with the most precise lattice determinations available.

In order to efficiently calculate renormalization parameters at two loops, we implemented a mixed approach, combining quenched high-β simulation with automated lattice perturbation theory. We were also able to extract estimates of the three-loop quenched contributions to the energy shift from high-β simulations and found that all perturbative coefficients are well behaved. The reliable

extraction of the two-loop energy shift convincingly demonstrates the effectiveness of our approach.

As part of this calculation, we also determined the fermionic contributions to the two-loop tadpole improvement factor for both the Landau and plaquette tadpole definitions.

We undertook a number of checks of both the automated lattice perturbation theory and the high-β simulations. For the former, we confirmed that we could reproduce published one-loop results, that the energy shift was infrared finite, and that the fermionic insertions in the gluon propagator obeyed the relevant Ward identity. For the latter, we were able to compare one-loop results to the exact finite-size perturbation theory results to ensure the correctness of our fits.

The uncertainty in our result is now dominated by the unknown fermionic contributions to the three-loop energy shift, which is, in principle, calculable with automated lattice perturbation theory. Greater statistics in the high-β simulations may also allow us to extract the quenched contributions to the mass renormalization with sufficient precision to enable an independent determination of the b-quark mass by direct matching.

APPENDIX A: FINITE VOLUME PERTURBATION THEORY

Without loss of generality, we consider a scalar model that is sufficient to demonstrate the approach. We take the NRQCD evolution for the heavy quark Green function to be

$$\tilde{G}(\boldsymbol{p}, t) = \tilde{K}(\boldsymbol{p}, t - 1)\tilde{G}(\boldsymbol{p}, t - 1), \qquad (A1)$$

where

$$\tilde{K}(\boldsymbol{p}, t) = \tilde{K}_0(\boldsymbol{p}, t)\left(1 - \frac{g}{2}\phi\right),$$
$$\tilde{K}_0(\boldsymbol{p}) = \left(1 - \frac{p^2}{2mn}\right)^n. \qquad (A2)$$

Here $K(\boldsymbol{x}, t)$ is the approximation to the evolution operator e^{-H} with

$$H = \left(1 + \frac{\nabla^2}{2m} - g\phi\right). \quad (A3)$$

We then have that

$$\tilde{G}_0(\boldsymbol{p}, t) = \tilde{K}(\boldsymbol{p})^t, \quad \text{with} \quad \tilde{G}_0(\boldsymbol{p}, 0) = 1. \quad (A4)$$

The diagram we consider is the rainbow diagram. The vertices are labeled with $(\boldsymbol{p}, t)$ coordinates, appropriate for the Hamiltonian formalism. The vertices are separated by time τ. The rainbow diagram has $\tau > 0$, while the associated tadpole diagram has $\tau = 0$. There is no effect of finite T on the calculation of the tadpole diagram, which is therefore given by finite-L Feynman perturbation theory. At $O(g^2)$ from the diagram we have the contribution

$$\tilde{G}_2(\boldsymbol{p}, t) = g^2 \sum_{\boldsymbol{q}, \tau=1}^{T-1} (t - \tau) \tilde{K}_0(\boldsymbol{p})^{t-\tau} \Gamma(\boldsymbol{q}, \tau) \tilde{K}_0(\boldsymbol{p} - \boldsymbol{q})^\tau. \quad (A5)$$

The factor $(t - \tau)$ is the number of temporal positions the graph can adopt, and $\Gamma(\boldsymbol{q}, \tau)$ is the ϕ-field propagator, given by

$$\Gamma(\boldsymbol{q}, \tau) = \frac{1}{T} \sum_{\Omega=0}^{T-1} \tilde{\Gamma}(\boldsymbol{q}, q_0) e^{iq_0\tau},$$
$$\tilde{\Gamma}(\boldsymbol{q}, q_0) = \frac{1}{\hat{q}^2 + \hat{q}_0^2 + \mu^2}, \quad (A6)$$

where

$$q_0 = \frac{2\pi\Omega}{T}, \qquad \hat{q}_0 = 2\sin\frac{q_0}{2},$$
$$q_i = \frac{2\pi Q_i}{L}, \qquad \hat{q}_i = 2\sin\frac{q_i}{2}, \quad (A7)$$

with $0 \le \Omega < T$ and $0 \le Q_i < L$. Then the contribution from the rainbow diagram is

$$\tilde{G}_2(\boldsymbol{p}, t) = \tilde{K}_0(\boldsymbol{p})^t g^2 \left[\frac{1}{L^3 T} \sum_{Q_i, \Omega} \sum_{\tau=1}^{t} (t - \tau) \right.$$
$$\left. \times \tilde{\Gamma}(\boldsymbol{q}, q_0) \left[e^{iq_0} \frac{\tilde{K}_0(\boldsymbol{p} - \boldsymbol{q})}{\tilde{K}_0(\boldsymbol{p})} \right]^\tau \right]. \quad (A8)$$

We now let

$$R(\boldsymbol{p}, q) = \left[e^{iq_0} \frac{\tilde{K}_0(\boldsymbol{p} - \boldsymbol{q})}{\tilde{K}_0(\boldsymbol{p})} \right], \quad (A9)$$

where $q \equiv (q_0, \boldsymbol{q})$. Then, using Eq. (A4), the one-loop rainbow diagram correction to the Green function is

$$\tilde{G}(\boldsymbol{p}, t) = [1 - g^2 A(\boldsymbol{p}, t)t + g^2 B(\boldsymbol{p}, t)] G_0(\boldsymbol{p}, t)$$
$$\sim [1 + g^2 B(\boldsymbol{p}, t)] e^{-g^2 A(\mathbf{p}, t)t} G_0(\boldsymbol{p}, t), \quad (A10)$$

and we deduce that $E_0^{(1)}(L, T, t) = g^2 A(0, t)$ and $Z_\psi^{(1)}(L, T, t) = g^2 B(0, t)$. Note that both $E_0^{(1)}$ and $Z_\psi^{(1)}$ depend on t but that for t sufficiently large both quantities will approach their asymptotic value. We then have

$$E_0^{(1)}(L, T, t) = -g^2 \frac{1}{L^3 T} \sum_{Q_i, \Omega} \sum_{\tau=1}^{t} \tilde{\Gamma}(\boldsymbol{q}, q_0) R(0, q)^\tau, \quad (A11)$$

$$Z_\psi^{(1)}(L, T, t) = g^2 \frac{1}{L^3 T} \sum_{Q_i, \Omega} \sum_{\tau=1}^{t} \tau \tilde{\Gamma}(\boldsymbol{q}, q_0) R(0, q)^\tau. \quad (A12)$$

We first consider $E_0^{(1)}(L, T, t)$. We carry out the geometrical sum and find

$$A(\boldsymbol{p}, t) = -g^2 \frac{1}{L^3 T} \sum_{Q_i, \Omega} \tilde{\Gamma}(\boldsymbol{q}, q_0) \frac{R(\boldsymbol{p}, q)}{1 - R(\boldsymbol{p}, q)} (1 - R(\boldsymbol{p}, q)^t). \quad (A13)$$

For $|R(0, q)| < 1$, for $\boldsymbol{q}$, the limits $T \to \infty$, $t \to \infty$ can be taken. We have that

$$\frac{R(\boldsymbol{p}, q)}{1 - R(\boldsymbol{p}, q)} = \frac{\tilde{K}_0(\boldsymbol{p} - \boldsymbol{q})}{e^{i(p_0 - q_0)} - \tilde{K}_0(\boldsymbol{p} - \boldsymbol{q})}$$
$$= e^{i(p_0 - q_0)} \tilde{K}_0(\boldsymbol{p} - \boldsymbol{q}) \tilde{G}_0(\boldsymbol{p} - \boldsymbol{q}), \quad (A14)$$

where we have used the on-shell condition for the external quark: $e^{ip_0} = \tilde{K}_0(\boldsymbol{p})$. In this limit we find

$$A(\boldsymbol{p}, \infty) = -g^2 \frac{1}{2i\pi L^3} \sum_{Q_i} \int_{|z|=1} \frac{dz}{z} e^{-i(p_0 - q_0)}$$
$$\times \tilde{K}_0(\boldsymbol{p} - \boldsymbol{q}) \tilde{G}_0(\omega, \boldsymbol{p} - \boldsymbol{q}), \quad (A15)$$

where $\omega = e^{i(p_0 - q_0)}$, with $z = e^{-iq_0}$, and the integral is over the unit circle in the complex z plane. This is the expression for the rainbow diagram derived from the NRQCD Feynman rules applicable in the limits $T \to \infty$, $t \to \infty$.

We conclude that, to account for the effect of finite temporal extent of the lattice in the perturbation theory, we make the replacement

$$\tilde{G}_0(\omega, \boldsymbol{p} - \boldsymbol{q}) \to \tilde{G}_0(\omega, \boldsymbol{p} - \boldsymbol{q})[1 - R(\boldsymbol{p}, q)^t] \quad (A16)$$

for the internal quark propagator and carry out the sums over the discrete values of $\boldsymbol{q}$ and q_0. There remains the choice for the value of t in this expression. We found that the results were insensitive to this choice as long as t was not close to either 0 or T, and so we chose $t = T/2$ for our calculations. $R(\boldsymbol{p}, q)$ is computed automatically by a numerical search for the poles of the external and internal propagators which gives $\tilde{K}_0(\boldsymbol{p})$ and $\tilde{K}_0(\boldsymbol{p} - \boldsymbol{q})$. For $E_0^{(1)}(L, T, t)$ we set $\boldsymbol{p} = 0$.

The wavefunction renormalization $Z_\psi^{(1)}$ is given by

$$Z_\psi^{(1)}(L, T, t) = ig^2 \frac{\partial}{\partial p0} \frac{1}{L^3 T} \sum_{Q_i, \Omega} \sum_{\tau=1}^{t} \tilde{\Gamma}(\boldsymbol{q}, q_0)$$
$$\times [e^{i(p_0 - q_0)} \tilde{K}_0(\boldsymbol{p} - \boldsymbol{q})]^\tau, \quad (A17)$$

evaluated on shell: $e^{-ip_0} = \tilde{K}_0(\boldsymbol{p})$. This is the usual formula applied to our augmented Feynman rule, and the derivative is computed using our automated TAYLOR derivative procedure.

In some cases we can have $|R| > 1$. This is the situation for some values of $\boldsymbol{q}$ given $\boldsymbol{p}$ and certainly occurs in moving NRQCD (mNRQCD) [63]. Because NRQCD is in the Hamiltonian formalism the value of t in Eq. (A8) is finite and the singularity in the quark propagator is removable. The poles in the gluon propagator are at $z = z_\pm$ with $|z_\pm| \gtrless 1$ and $z_+ z_- = 1$. Schematically, Eq. (A15) takes the form

$$A(\boldsymbol{p}) = C \sum_{Q_i} \int_{|z|=1} dz \frac{1}{z - z_-} \frac{1}{z - z_+} \frac{z(1 - (a/z)^t)}{z - a} \quad (A18)$$

where C is a constant and $a = \tilde{K}_0(\boldsymbol{p} - \boldsymbol{q})/\tilde{K}_0(\boldsymbol{p})$. The integration contour is $|z| = 1$ and is determined by the formalism; no distortion is available in the NRQCD evolution to avoid pole crossing. However, the singularity at $z = a$ is removable, and so there is no issue of it crossing the contour. The integration is done by Cauchy's theorem at the $z = z_+$ pole, and the factor from the geometric summation is then evaluated to be $(1 - (a/z_+)^t)$; the need to consider the pole of order $(t - 1)$ at the origin is then avoided. Since $|a| < |z_+|$ the limit $t \to \infty$ can now be taken. This corresponds to the usual rule for analytic continuation in the calculation of the Feynman diagram, where the radius $|z|$ of the contour is increased to avoid crossing by the quark pole at $z = a$.

APPENDIX B: GENERATING CONFIGURATIONS AND GAUGE FIXING

1. Langevin Markov chain configurations

Configurations for the Monte Carlo simulations are generated with a Markov chain that is updated via a Langevin algorithm. The Langevin method treats the Markov chain as a classical path in phase space, using the action as a potential to enforce the Boltzmann distribution. Using the notation of Sec. III B, the Langevin equation is given by

$$\frac{\partial \tilde{U}}{\partial \tau} = -\frac{\partial S}{\partial \tilde{U}} + \eta, \quad (B1)$$

where S is the action, η is a random noise term, and τ is the distance along the path. Using the Fokker-Plank equation it can be shown that this path will sample the configuration space with probability density

$$P(\tilde{U}) = e^{-S[\tilde{U}]}, \quad (B2)$$

the Boltzmann distribution, as desired.

As Eq. (B1) is an initial value problem, its solution can be approximated via an iterative method, where the derivative on the left-hand side is written as a finite difference, with step size ϵ. This introduces step-size errors in the action so that the distribution that is simulated is altered to

$$\bar{P}(\tilde{U}) = e^{-\bar{S}[\tilde{U}, \epsilon]}, \quad (B3)$$

where $\bar{S}[\tilde{U}, \epsilon]$ is the simulated action which is expansible as

$$\bar{S}[\tilde{U}, \epsilon] = S + \epsilon S_1 + \epsilon^2 S_2 + \cdots. \quad (B4)$$

The step-size errors in Eq. (B4) can be systematically eliminated using higher-order approximations to the derivative in Eq. (B1). In this work a second-order Runge-Kutta algorithm (RK2) which eliminates $\mathcal{O}(\epsilon)$ errors was used. This is implemented as a midpoint method adapted to diffusion on a group manifold [64].

Simulations were run with a step size $\epsilon = 0.2$. Analysis shows that ϵ scaling errors are of the order $\approx 0.05\%$. Autocorrelation times were measured to be of the order of 5–10 (25–50 updates) for the plaquette and 10–20 (50–100 updates) for the twisted Polyakov loop [10]. Here 100 configurations were skipped between measurements. For each value of β_{pl} on each lattice size, 32 independent Markov chains were generated. Each chain produced 128 configurations (4096 configurations in total).

2. Gauge fixing with twisted boundaries

Configurations generated from the Markov chain have the gauge freedom described in Eq. (24). This can be fixed by the application of a gauge condition. In this work we wish to fix the configurations to Coulomb gauge. In the continuum Coulomb gauge is achieved by the gauge transformation that satisfies

$$\partial_i A_i^g = 0. \quad (B5)$$

On the lattice this corresponds to maximizing the quantity

$$W[g] = \sum_{x,i=1}^{3} \Big[g(\boldsymbol{x}) \tilde{U}_i(\boldsymbol{x}) g^\dagger(\boldsymbol{x} + \boldsymbol{e}_i)$$
$$- \frac{1}{16} g(\boldsymbol{x}) \tilde{U}_i(\boldsymbol{x}) \tilde{U}_i(\boldsymbol{x} + \boldsymbol{e}_i) g^\dagger(\boldsymbol{x} + 2\boldsymbol{e}_i) \Big], \quad (B6)$$

with respect to the gauge transform field $g(\boldsymbol{x})$ for each time slice. This is $\mathcal{O}(a^2)$ improved [65]. The maximization is performed via a conjugate-gradient method, using a backtrack line search. Each time slice is gauge fixed separately. Errors due to numerical maximization are estimated to be insignificant.

Fixing to Coulomb gauge leaves an ambiguity, since it is possible to construct an additional purely temporal gauge transformation

$$\tilde{U}_4(\boldsymbol{x}, t) \to \tilde{U}_4^{g^{(T)}}(x) = g^{(T)}(t)\tilde{U}_4(\boldsymbol{x})g^{(T)\dagger}(t+1). \quad \text{(B7)}$$

This gauge transformation must obey the twisted boundary conditions

$$g^{(T)}(t) = \Omega_i g^{(T)}(t)\Omega_i^\dagger, \quad \text{(B8)}$$

for $i = 1, 2, 3$. The only solutions are

$$g^{(T)} = \mathbb{1}z^n, \quad \text{(B9)}$$

for $n = 0, \ldots, N_c$, where z is given in (22).

After fixing to Coulomb gauge, each time may be in a different gauge. In order to measure time-dependent operators, the time slices must all be in the same gauge. The gauges are all fixed to be the same as that on the first time slice. Since the gauge transformations in (B9) form a group, this is achieved by applying an additional transformation. The gauge transformation on the first time slice is set to the unit matrix,

$$g^{(T)}(t = 0) = \mathbb{1}. \quad \text{(B10)}$$

The transformations on subsequent time slices are chosen sequentially to maximize

$$\text{Re}[\text{Tr}g^{(T)}(t-1)\tilde{U}_4(\boldsymbol{0}, t-1)g^{(T)\dagger}(t)], \quad \text{(B11)}$$

for $t = 1, \ldots T - 1$.

APPENDIX C: $\overline{\text{MS}}$ MATCHING FORMULAS

The relation between α_V and $\alpha_{\overline{\text{MS}}}$ is given by [49,54,55]

$$\alpha_V = \alpha_{\overline{\text{MS}}}(1.0 + c_0\alpha_{\overline{\text{MS}}} + c_1\alpha_{\overline{\text{MS}}}^2). \quad \text{(C1)}$$

The coefficients are

$c_0 = (a_1 + \beta_0 \log(x))/4\pi,$

$c_1 = (a_2 + (\beta_0 \log(x))^2 + (\beta_1 + 2\beta_0 a_1) \log(x))/(4\pi)^2,$

with $\log(x) = 0$, since both couplings are evaluated at the same scale,

$$\beta_0 = 11 - 2n_f/3, \quad \text{(C2)}$$

$$\beta_1 = 2(51 - 19n_f/3), \quad \text{(C3)}$$

$$a_1 = (31C_a - 20T_f n_f)/9, \quad \text{(C4)}$$

$$a_2 = \left(\frac{4343}{162} + 4\pi^2 - \pi^4/4 + 22\zeta(3)/3\right)C_a^2$$
$$- \left(\frac{1798}{81} + 56\zeta(3)/3\right)C_a T_f n_f$$
$$- \left(\frac{55}{3} - 16\zeta(3)\right)C_f T_f n_f + \frac{400}{81}T_f^2 n_f^2. \quad \text{(C5)}$$

Note the discrepancy between [49,54].

The pole to $\overline{\text{MS}}$ renormalization is calculated to three loops in [16]

$$M_b^{\text{pole}} = Z_M(\bar{m}_b)\bar{m}_b(\bar{m}_b), \quad \text{(C6)}$$

with

$$Z_M(\bar{m}_b) = 1 + \frac{4}{3}\frac{\alpha_{\overline{\text{MS}}}(\bar{m}_b)}{\pi}$$
$$+ \left(\frac{\alpha_{\overline{\text{MS}}}(\bar{m}_b)}{\pi}\right)^2(-1.0414n_f + 13.4434)$$
$$+ \left(\frac{\alpha_{\overline{\text{MS}}}(\bar{m}_b)}{\pi}\right)^3(0.6527n_f^2 - 26.655n_f + 190.595).$$
$$\quad \text{(C7)}$$

We actually need the inverse of this series, which we define as the three-loop approximation to $1/Z_M$. With $n_f = 3$ this is

$$Z_M^{-1}(\bar{m}_b) = 1 - 0.42441318\alpha_{\overline{\text{MS}}}$$
$$- 0.86542701\alpha_{\overline{\text{MS}}}^2 - 2.94639\alpha_{\overline{\text{MS}}}^3. \quad \text{(C8)}$$

The $\overline{\text{MS}}$ coupling is discontinuous at quark mass thresholds since the heavy mass quarks are explicitly decoupled by matching to a theory with a different number of flavors. The formula for matching the n_f theory to a theory with $n_l = n_f - 1$ flavors at the threshold is [58]

$$\alpha_{\overline{\text{MS}}}^{(n_l)} = \alpha_{\overline{\text{MS}}}^{(n_f)}\left(1 + \frac{c_2}{\pi^2}\left(\alpha_{\overline{\text{MS}}}^{(n_f)}\right)^2 + \frac{c_3}{\pi^3}\left(\alpha_{\overline{\text{MS}}}^{(n_f)}\right)^3\right), \quad \text{(C9)}$$

with everything evaluated at the threshold scale of the n_f theory and the coefficients

$$c_2 = \frac{11}{72}, \quad \text{(C10)}$$

$$c_3 = \frac{82043}{27648}\zeta(3) + \frac{564731}{124416} - \frac{2633}{31104}n_l. \quad \text{(C11)}$$

Crossing thresholds for a running mass in a mass-independent scheme gives the same difficulties as the coupling. The relation between the n_l flavor effective theory and the n_f flavor theory for the $\overline{\text{MS}}$ running mass at the threshold is [66]

$$m^{(n_l)} = m^{(n_f)}\left(1 + \frac{0.2060}{\pi^2}\left(\alpha_{\overline{\text{MS}}}^{(n_f)}\right)^2$$
$$+ \frac{(1.8476 + 0.0247n_l)}{\pi^3}\left(\alpha_{\overline{\text{MS}}}^{(n_f)}\right)^3\right). \quad \text{(C12)}$$

For the inverse of these operations we include higher-order terms so that it reproduces the original value to better accuracy.

[1] K. Chetyrkin, J. Kuhn, A. Maier, P. Maierhofer, P. Marquard, M. Steinhauser, and C. Sturm, Phys. Rev. D **80**, 074010 (2009).

[2] S. Narison, Phys. Lett. B **707**, 259 (2012).

[3] S. Narison, Phys. Lett. B **706**, 412 (2012).

[4] I. Allison *et al.* (HPQCD Collaboration), Phys. Rev. D **78**, 054513 (2008).

[5] C. McNeile, C. T. H. Davies, E. Follana, K. Hornbostel, and G. P. Lepage, Phys. Rev. D **82**, 034512 (2010).

[6] B. A. Thacker and G. P. Lepage, Phys. Rev. D **43**, 196 (1991).

[7] G. P. Lepage, L. Magnea, C. Nakhleh, U. Magnea, and K. Hornbostel, Phys. Rev. D **46**, 4052 (1992).

[8] A. Gray, I. Allison, C. Davies, E. Gulez, G. Lepage, J. Shigemitsu, and M. Wingate, Phys. Rev. D **72**, 094507 (2005).

[9] W. Dimm, G. P. Lepage, and P. B. Mackenzie, Nucl. Phys. B, Proc. Suppl. **42**, 403 (1995).

[10] A. Hart, R. R. Horgan, and L. C. Storoni, Phys. Rev. D **70**, 034501 (2004).

[11] E. H. Mueller *et al.*, Proc. Sci., LAT2009 (2009) 241.

[12] I. Bigi and N. Uraltsev, Phys. Lett. B **321**, 412 (1994).

[13] M. Beneke and V. M. Braun, Nucl. Phys. **B426**, 301 (1994).

[14] G. T. Bodwin and Y.-Q. Chen, Phys. Rev. D **60**, 054008 (1999).

[15] C. T. H. Davies, K. Hornbostel, A. Langnau, G. Lepage, A. Lidsey, C. Morningstar, J. Shigemitsu, and J. Sloan, Phys. Rev. Lett. **73**, 2654 (1994).

[16] K. Melnikov and T. van Ritbergen, Phys. Lett. B **482**, 99 (2000).

[17] R. J. Dowdall *et al.*, Phys. Rev. D **85**, 054509 (2012).

[18] J. Daldrop, C. Davies, and R. Dowdall (HPQCD Collaboration), Phys. Rev. Lett. **108**, 102003 (2012).

[19] R. Dowdall, C. Davies, T. Hammant, and R. Horgan, Phys. Rev. D **86**, 094510 (2012).

[20] E. B. Gregory, C. T. Davies, I. D. Kendall, J. Koponen, K. Wong *et al.*, Phys. Rev. D **83**, 014506 (2011).

[21] R. Dowdall, C. Davies, R. Horgan, C. Monahan, and J. Shigemitsu (HPQCD Collaboration), arXiv:1302.2644.

[22] S. J. Brodsky, G. P. Lepage, and P. B. Mackenzie, Phys. Rev. D **28**, 228 (1983).

[23] M. Lüscher and P. Weisz, Phys. Lett. **158B**, 250 (1985).

[24] M. Alford, W. Dimm, G. P. Lepage, G. Hockney, and P. B. Mackenzie, Phys. Lett. B **361**, 87 (1995).

[25] A. Bazavov, D. Toussaint, C. Bernard, J. Laiho, C. DeTar *et al.*, Rev. Mod. Phys. **82**, 1349 (2010).

[26] G. P. Lepage, Phys. Rev. D **59**, 074502 (1999).

[27] C. Aubin, C. Bernard, C. DeTar, J. Osborn, S. Gottlieb, E. Gregory, D. Toussaint, U. Heller, J. Hetrick, and R. Sugar, Phys. Rev. D **70**, 094505 (2004).

[28] A. Hart, G. M. von Hippel, R. R. Horgan, and L. C. Storoni, J. Comput. Phys. **209**, 340 (2005).

[29] A. Hart, G. M. von Hippel, R. R. Horgan, and E. H. Müller, Comput. Phys. Commun. **180**, 2698 (2009).

[30] I. T. Drummond, A. Hart, R. R. Horgan, and L. C. Storoni, Phys. Rev. D **66**, 094509 (2002).

[31] I. T. Drummond, A. Hart, R. R. Horgan, and L. C. Storoni, Nucl. Phys. B, Proc. Suppl. **119**, 470 (2003).

[32] I. T. Drummond, A. Hart, R. R. Horgan, and L. C. Storoni, Phys. Rev. D **68**, 057501 (2003).

[33] A. Hart, G. M. von Hippel, and R. R. Horgan, Phys. Rev. D **75**, 014008 (2007).

[34] E. H. Mueller, A. Hart, and R. R. Horgan, Phys. Rev. D **83**, 034501 (2011).

[35] T. C. Hammant, A. G. Hart, G. M. von Hippel, R. R. Horgan, and C. J. Monahan, Phys. Rev. Lett. **107**, 112002 (2011).

[36] G. Lepage, J. Comput. Phys. **27**, 192 (1978).

[37] G. M. von Hippel, Comput. Phys. Commun. **181**, 705 (2010).

[38] E. Gulez, J. Shigemitsu, and M. Wingate, Phys. Rev. D **69**, 074501 (2004).

[39] M. A. Nobes, H. D. Trottier, G. P. Lepage, and Q. Mason, Nucl. Phys. B, Proc. Suppl. **106-107**, 838 (2002).

[40] E. H. Müller, Ph.D. thesis, University of Edinburgh, 2009.

[41] Q. Mason, Ph.D. thesis, Cornell University, 2004.

[42] M. Luscher, Nucl. Phys. **B219**, 233 (1983).

[43] G. 't Hooft, Nucl. Phys. **B153**, 141 (1979).

[44] M. Lüscher and P. Weisz, Nucl. Phys. **B266**, 309 (1986).

[45] H. Trottier, N. Shakespeare, G. Lepage, and P. Mackenzie, Phys. Rev. D **65**, 094502 (2002).

[46] K. Hornbostel, G. Lepage, and C. Morningstar, Phys. Rev. D **67**, 034023 (2003).

[47] Q. Mason, H. Trottier, C. Davies, K. Foley, A. Gray, G. Lepage, M. Nobes, and J. Shigemitsu (HPQCD Collaboration and UKQCD Collaboration), Phys. Rev. Lett. **95**, 052002 (2005).

[48] K. Y. Wong, H. D. Trottier, and R. Woloshyn, Phys. Rev. D **73**, 094512 (2006).

[49] Y. Schroder, Phys. Lett. B **447**, 321 (1999).

[50] C. Davies, E. Follana, I. Kendall, G. P. Lepage, and C. McNeile (HPQCD Collaboration), Phys. Rev. D **81**, 034506 (2010).

[51] T. Hammant, A. Hart, G. von Hippel, R. Horgan, and C. Monahan, Phys. Rev. Lett. **107**, 112002 (2011).

[52] E. Follana, Q. Mason, C. Davies, K. Hornbostel, G. Lepage, J. Shigemitsu, H. Trottier, and K. Wong (HPQCD Collaboration), Phys. Rev. D **75**, 054502 (2007).

[53] G. P. Lepage, B. Clark, C. T. H. Davies, K. Hornbostel, P. B. Mackenzie, C. Morningstar, and H. Trottier, Nucl. Phys. B, Proc. Suppl. **106-107**, 12 (2002).

[54] M. Peter, Phys. Rev. Lett. **78**, 602 (1997).

[55] M. Peter, Nucl. Phys. **B501**, 471 (1997).

[56] Y. Schroeder, Phys. Lett. B **447**, 321 (1999).

[57] G. Prosperi, M. Raciti, and C. Simolo, Prog. Part. Nucl. Phys. **58**, 387 (2007).

[58] K. Chetyrkin, B. A. Kniehl, and M. Steinhauser, Phys. Rev. Lett. **79**, 2184 (1997).

[59] T. van Ritbergen, J. Vermaseren, and S. Larin, Phys. Lett. B **400**, 379 (1997).

[60] F. Bernardoni, B. Blossier, J. Bulava, M. Della Morte, P. Fritzsch *et al.*, arXiv:1210.6524.

[61] P. Dimopoulos *et al.* (ETM Collaboration), J. High Energy Phys. 01 (2012) 046.

[62] J. Beringer *et al.*, J. Phys. D **86**, 010001 (2012).

[63] R. R. Horgan *et al.*, Phys. Rev. D **80**, 074505 (2009).

[64] S. Catterall, I. Drummond, and R. Horgan, Phys. Lett. B **254**, 177 (1991).

[65] G. Lepage, B. Clark, C. T. H. Davies, K. Hornbostel, P. B. Mackenzie, C. Morningstar, and H. Trottier, Nucl. Phys. B, Proc. Suppl. **106-107**, 12 (2002).

[66] K. Chetyrkin, B. A. Kniehl, and M. Steinhauser, Nucl. Phys. **B510**, 61 (1998).

[67] S. Bodenstein, J. Bordes, C. Dominguez, J. Penarrocha, and K. Schilcher, Phys. Rev. D **85**, 034003 (2012).

[68] A. Laschka, N. Kaiser, and W. Weise, Phys. Rev. D **83**, 094002 (2011).

[69] R. Boughezal, M. Czakon, and T. Schutzmeier, Phys. Rev. D **74**, 074006 (2006).

[70] O. Buchmuller and H. Flacher, Phys. Rev. D **73**, 073008 (2006).

[71] A. Pineda and A. Signer, Phys. Rev. D **73**, 111501 (2006).

[72] C. W. Bauer, Z. Ligeti, M. Luke, A. V. Manohar, and M. Trott, Phys. Rev. D **70**, 094017 (2004).

[73] A. Hoang and M. Jamin, Phys. Lett. B **594**, 127 (2004).

[74] J. Bordes, J. Penarrocha, and K. Schilcher, Phys. Lett. B **562**, 81 (2003).

[75] G. Corcella and A. Hoang, Phys. Lett. B **554**, 133 (2003).

[76] M. Eidemuller, Phys. Rev. D **67**, 113002 (2003).

[77] J. Erler and M. xing Luo, Phys. Lett. B **558**, 125 (2003).

[78] N. Brambilla, Y. Sumino, and A. Vairo, Phys. Rev. D **65**, 034001 (2002).

[79] A. A. Penin and M. Steinhauser, Phys. Lett. B **538**, 335 (2002).

[80] A. Hoang, P. Ruiz-Femenia, and M. Stahlhofen, J. High Energy Phys. 10 (2012) 188.